博士学位論文

Scanning structured-illumination microscopy with spectral and non-linear imaging techniques

走査型構造化照明を用いた分光および非線形イメージング法

渡辺　梢

2015 年 12 月

大阪大学大学院工学研究科

Table of contents

Introduction

Recent developments in fluorescence microscopy have enabled us to improve the spatial resolution in optical imaging beyond the diffraction barrier given by the wave nature of light. Controlling the emission capability of fluorescent probes labeling a sample by stimulated emission or photoactivation is the key to achieve a spatial resolution of a few tens of nanometers. Although this approach has a high potential to revolutionize biological imaging, it is not applicable to all types of optical microscopy. Label-free imaging techniques, such as Raman microscopy or harmonic generation microscopy, do not rely on fluorescence labeling to make the image contrast; hence, the above approach cannot be utilized for such microscopies. Even in fluorescence imaging, there are situations, such as in deep-tissue imaging, where precise control of the fluorescence emission capability is quite difficult. Therefore, the spatial resolution of such imaging techniques has been still limited to that of classical light microscopy. The realization of high-resolution chemical imaging and deep-tissue imaging is highly desired because of its expectedly strong scientific, medical, and industrial importance.

In this thesis, I present the development of new microscopy techniques that combine laser scanning microscopy with structured illumination microscopy (SIM) in order to realize high-resolution label-free imaging and deep-tissue imaging. SIM improves the spatial resolution by using spatially patterned illumination light to effectively increase the resolving power of the microscope without relying on the optical responses of fluorescent probes. By introducing structured illumination in laser scanning microscopy, it is possible to implement high-resolution spectroscopical and non-linear excitation techniques to expand the availability of high-resolution microscopy. I applied this concept to Raman microscopy in order to improve the spatial resolution in label-free imaging. I also implemented structured illumination in two-photon excitation microscopy for high-resolution deep-tissue imaging.

For the realization of label-free high-resolution imaging, I developed structured line illumination Raman microscopy. Sample is illuminated with a structured line pattern, and the Raman scattering from each point is observed using a slit-spectrometer. The obtained spatial pattern is mathematically processed in Fourier space to extract the high spatial resolution information at every wavenumber in parallel. I applied the technique to the observation of different kinds of specimens: polymer nanoparticles, graphene, graphite, and mouse brain tissue. The experimental result showed that spatial resolution in the slit direction is twice higher than

that of conventional slit-scanning Raman microscopy.

Two-photon excitation by NIR laser pulses was incorporated with the developed structured illumination microscope toward high-resolution deep-tissue imaging. The sample is illuminated with a structured spot rather than wide-field illumination. The spot diameter was 5-10 μm, which produces intense excitation light for two-photon excitation. An imaging theory treating the imaging characteristics of the structured spot illumination is presented. The improvement of spatial resolution in structured spot illumination is experimentally confirmed by the observation of fluorescence nanoparticles. This result indicates the possibility of high-resolution two-photon imaging of deep tissues of biological samples.

This dissertation is divided into three parts. In chapter 1, for the first part of the thesis, I introduce the overview of current microscopy techniques to overcome the physical limit of the spatial resolution in optical imaging. Among the several high-resolution optical imaging techniques, I especially discuss SIM, which provides high-speed and relatively high-resolution optical imaging capability. For the second part of the thesis, the application of the SIM to Raman microscopy is discussed. The imaging characteristic of structured line illumination microscopy is discussed in chapter 2, and the development of structured line illumination Raman microscopy and its experimental results are shown in chapter 3. For the last part of the thesis, the application of the SIM to two-photon microscopy is discussed. In chapter 4, theoretical spatial resolution and its imaging characteristics are discussed. In chapter 5, I present the development and the experimental results of the spot-SIM are presented.

Chapter 1
The approaches for the high-resolution optical imaging

In this chapter, I discuss the microscopy techniques, which had been developed to achieve high spatial resolution optical imaging. First, I review the development of optical imaging methods up to the present, and the imaging theory. Also the high-resolution imaging techniques, which had been developed in these two decades, are briefly introduced. In chapter 1.2, I introduce the high-resolution imaging methods that utilize the non-linear optical responses or the optical switching reaction of the fluorophores. In chapter 1.3, I introduce the structured illumination microscopy (SIM), which enables high-speed and relatively high-resolution imaging.

1.1 Spatial resolution in optical imaging methods

Emergence of light microscopy

Optical microscopy is the imaging method to observe the interaction between the incident light and the sample. There are various optical microscopes to measure different kind of optical properties of the sample; such as transmission, reflection, absorption, scattering, fluorescence, polarization, phase retardation, and photo-thermal expansion. One of the characteristics is that the information of the molecule can be obtained, since visible wavelength light interacts with the molecule inside the object. Another advantage of the optical microscopy is non-invasive imaging capability. Therefore, even the biological imaging of intact living cell is possible. Largely because of the non-invasive imaging capability and its simplicity, optical microscopy is widely used in science, industry and medical fields.

The invention of the optical microscope was started with transmission microscopy in 16th century[1], and the other microscopy methods are invented afterwards. In the middle of the 19th century, Ernst Abbe built the diffraction theory, which is the first theoretical explanation of the optical microscopy resolution. He also contributed to the development of the industrial manufacture of optical microscopy with Carl Zeiss and Otto Schott. The optical design that is originated from the optical theory changed the practical optical design until then, and made great contribution to the improvement of the microscope. In the early 20th century, optical

microscopy experienced another great revolution – the invention of fluorescence microscopy. The invention of the fluorescence microscopy and the various kinds of fluorophores has opened up the possibility to determine the position of the each cellular organelle, which cannot be seen without staining with fluorescent molecule.

Another important invention in the microscopy design is the appearance of the confocal microscopy (Figure 1-1). In 1960s, scientists started to use pinhole before the point detector, and found that the out-of focus light can be largely suppressed by the effect of pinhole. David Egger built a pinhole-scanning microscope in 1967, and imaged the reflection light from brain and ganglion. The out-of-focus suppression is called optical sectioning, since it enables imaging of the sample sectioned in the depth of the sample. Today, confocal fluorescence microscopy is extensively used by biologists, for its capability to image the distribution of each cellular organelle inside the cell in few hundreds of nanometer resolution. In 1981, Collin Sheppard and Tony Willson proposed a systematical theory to treat the spatial resolution of the confocal microscopy. It is now generally used to understand the characteristics of various optical imaging techniques.

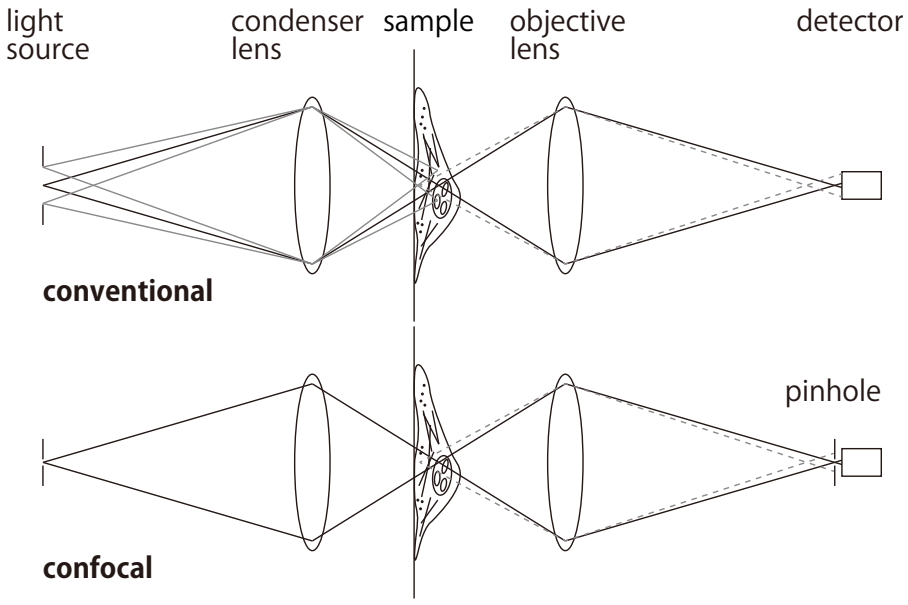

Fig. 1-1 The pinhole in front of the point detector prohibits the light from defocused area to contribute to the image.

Image formation and the spatial resolution in light microscopy

In this section, I introduce the brief ideas of imaging theory. The limit of the spatial resolution in the conventional microscopy is determined by the wave optics. Abbe's diffraction theory treats the image formation as the interference of the 0th order and 1st order diffraction light (Fig. 1-2). Here, assume that the sample is illuminated with on-axis coherent light source. The sample, which has the distribution of single spatial frequency, coherently diffracts the incident light. In the figure, different order of the diffraction is illustrated in different color. The diffraction light is then go through the imaging optics, and forms interference pattern at the image detector. The imaging of the arbitrary structured sample can be also treated in the same way, since any sample can be considered as the linear combination of the objects with single spatial frequency.

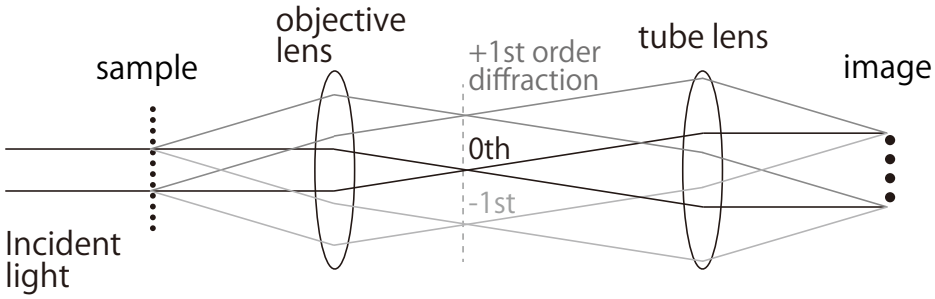

Fig. 1-2 Abbe's diffraction theory explains the image formation as the interference of coherently diffracted light by the sample structure.

The maximum angle of the diffraction light that can be collected by the objective lens limits the maximum spatial resolution in the system. The effective radius of the objective lens, ϱ_0, restricts the k vector that can transmit the lens (Fig. 1-3). The circle in the figure has the radius of the effective spatial frequency of the light in the medium, n/λ, with the refractive index of n. The objective lens with numerical aperture (NA) has the effective radius of NA/λ. NA is defined as $NA = n\sin\theta$, with and the maximum angle of the light which can pass through the lens (θ). Here, the diffraction light with the wave vector of k_1, that satisfies the following Bragg's diffraction equation, can transmit the lens.

$$K = k_1 - k_0$$

Therefore, in on-axis illumination case, the maximum spatial frequency of the sample, which can transmit the lens, is limited to $\sim\varrho_0$. The maximum spatial frequency that can be imaged in this system can be achieved by the oblique illumination. In the case of oblique illumination,

incident light illuminate the sample with the angle that is illustrated in the right figure in Fig. 1-3. Therefore, maximum spatial frequency of the sample that can be transmit the lens is $2\varrho_0 = 2NA/\lambda$.

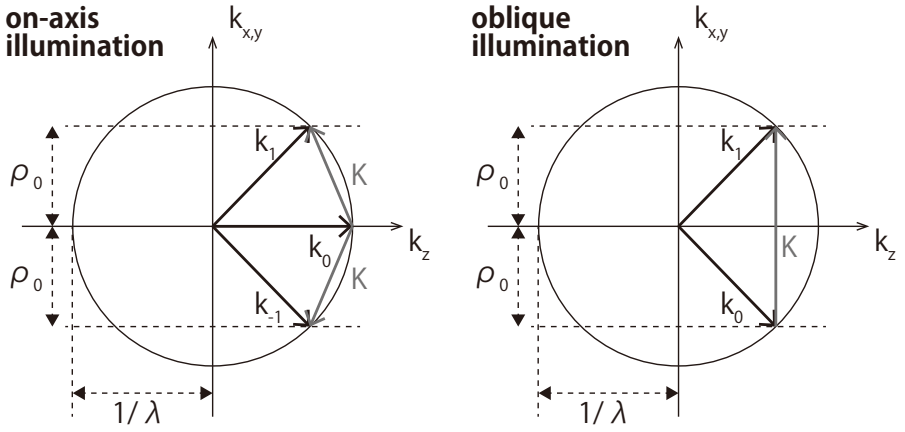

Fig. 1-3 Detectable spatial frequency information with on-axis illumination and oblique illumination explained in Ewalt sphere.

This maximum spatial frequency is the classical limitation of the spatial resolution, which corresponds to the diffraction limit, derived by Ernst Abbe. The imaging modality is called coherent detection, because the coherent interference of diffraction light forms an image. In contrast, if the light generated from the sample is incoherent, we have to consider different imaging modality. For example, the fluorescence from the different point of the sample is not coherent; therefore, it doesn't interfere mutually. Instead of the interference of the 0th order and 1st order diffraction light, fluorescence microscopy forms the image by the interference of the fluorescence itself (Fig. 1-4). Even if the fluorescence is generated at the infinitely small spot, the focus pattern created by the lens can not be infinitely small spot, since the diffraction of the light by a lens is treated as the Fresnel's diffraction by a circular aperture, thus it has the certain spot size. As shown in Fig. 1-4, we assume wide-field fluorescence system: light source illuminate the sample uniformly, and the fluorescence is detected using image detector. In this case, the finest structure that can be transferred through the wide-field microscopy system is the spatial frequency of $2NA/\lambda$, since the interference of the highest angle that can transmit the objective lens determine the resolution limit.

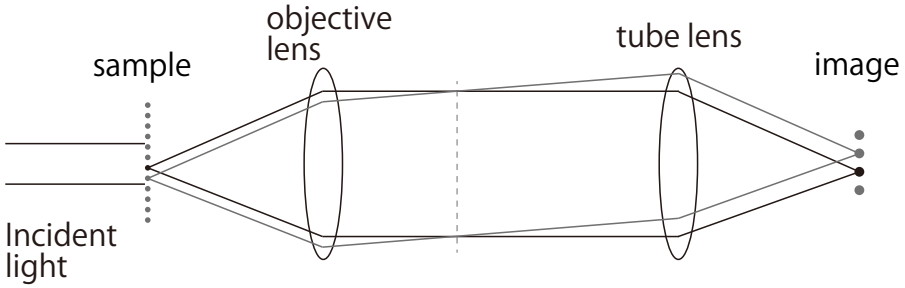

Fig. 1-4 Incoherent detection forms an image by the interference of the emission from the fluorescence itself.

The imaging characteristics of the optical microscopy are generally treated by the point spread function (PSF) and optical transfer function (OTF) or coherent transfer function (CTF), as introduced by C. Sheppard and T. Wilson. In the coherent imaging system, obtained amplitude image g(x) with the amplitude point spread function h(x) from the transmittance distribution of the sample f(x) is given as below.

$$g(x) = h(x) \otimes f(x) \tag{1-1}$$

Here, h(x) is the Fourier transformation of the transmittance distribution of the objective pupil. For the confocal microscopy system, the detection system should be also taken into account for the image formation. Suppose that the detection pinhole is infinitely small, the observed amplitude transmittance distribution image is given as

$$g(x) = h_1(x)h_2(x) \otimes f(x) \tag{1-2}$$

with the illumination amplitude point spread function of $h_1(x)$ and detection amplitude point spread function of $h_2(x)$. Here, the spatial frequency response of the whole system, CTF, is given as below with the objective pupil function of P_1 and P_2.

$$CTF = F.T.[h_1(x)h_2(x)] = P_1 \otimes P_2 \tag{1-3}$$

In the case of incoherent imaging, obtained intensity distribution g'(x) from the amplitude distribution of the light after the sample f'(x) is given as below.

$$g'(x) = |h(x)|^2 \otimes f'(x) \tag{1-4}$$

In the case of incoherent confocal microscopy system with infinitely small detection pinhole,

$$g(x) = |h_1(x)|^2|h_2(x)|^2 \otimes f'(x) \tag{1-5}$$

The spatial frequency response of the whole system, OTF, is given as below.

$$OTF = F.T.[|h_1(x)|^2|h_2(x)|^2] = [(P_1 \otimes P_1) \otimes (P_2 \otimes P_2)] \tag{1-6}$$

Using the PSF and OTF concept, it is practically useful to treat the whole system of the optical microscopy.

Super-resolution microscopy

The invention of the fluorescence microscopy had contributed to break the spatial resolution limit described above. In order to overcome the physical limitation of spatial resolution, the methods called “super-resolution imaging” had developed in these decades. The invention of the super-resolution microscopy began with STED (STimulated Emission Depletion) microscopy by Stephan Hell in 1994 [2]. After that, in 1999, Mats G. L. Gustafsson invented SIM (Structured Illumination Microscopy) that enables high spatial resolution imaging by illuminating sample with spatially structured pattern [3]. Another important inventions in super-resolution microscopy are PALM (PhotoActivated Localizatioin Microscopy) by Eric Betzig [4] and STORM (STochastic Optical Reconstruction Microscopy) by M. J. Rust [5], both in 2006. Now these new optical imaging techniques opened up the possibility to image the detailed structures inside the biological specimen, even in few nanometer levels. In addition, the application of the super-resolution imaging techniques nowadays expands to non-fluorescence samples [6]. The detailed characteristics of these approaches for high-resolution imaging are introduced in the following chapter.

1.2 Non-linear optical effects for resolution enhancement

Photoswitching for resolution enhancement

Photoswitching of the fluorophore has been used for the resolution enhancement in fluorescence microscopy. Although the smallest size of the spot by focusing light has the physical limitation, the fluorescence emission probability in the focus spot can be also controlled. One candidate is stimulated excitation emission. STED microscopy, which was awarded the Nobel Prize in 2014, utilizes stimulated emission for the resolution improvement. Another candidate is ground state depletion used in GSD microscopy [7]. These methods are currently classified under one super-resolution concept, RESOLFT (reversible saturable optically linear fluorescence transitions) microscopy [8], since both of these techniques use the transition between two different energy states for the resolution enhancement.

Here, I introduce the STED microscopy as an example. STED microscopy uses point-scanning microscopy system, and detects the fluorescence from the point illuminated by the excitation laser. The excitation beam illuminates the sample with diffraction limited focus spot as illustrated in Fig. 1-5. At the same time, donuts shaped STED beam are superposed on the same position of the sample, and the electrons in the excited state change the state to the ground state as a result of stimulated emission in the area illuminated with STED beam. The resultant fluorescence in the area is reduced. Therefore, the effective excitation area is smaller in STED microscopy, hence the enhanced spatial resolution. As illustrated in the figure, higher intensity of STED beam induces saturation of the stimulated emission; therefore, the effective excitation area can be reduced to the factor of few tens of nanometers.

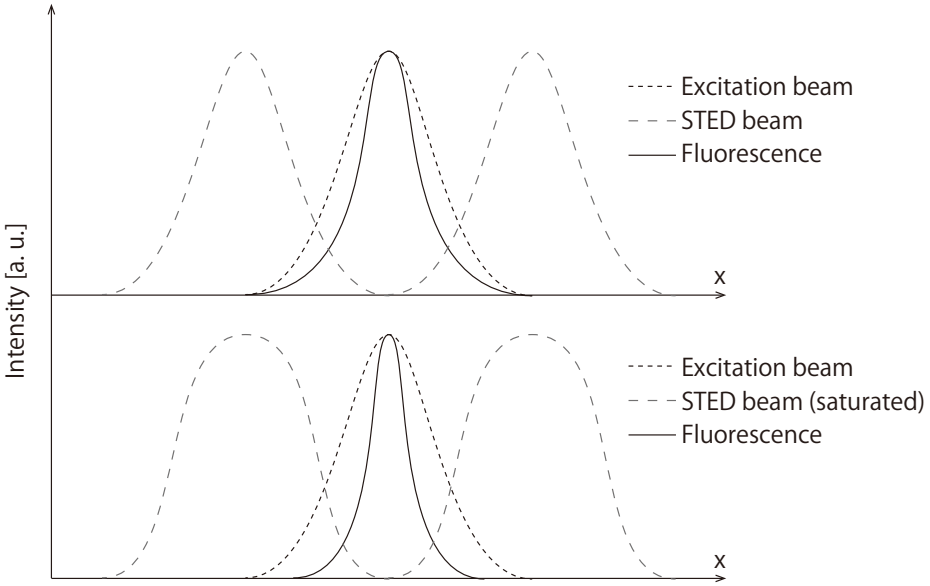

Fig. 1-5. The fluorescence emission area can be reduced by controlling the population of the electrons in the excited state with donuts-shaped STED beam.

Not only the stimulated emission, the concept of photo switching is applicable for any kinds of photo switching effect. Fig. 1-6 shows the energy diagrams that have used photo switching for resolution enhancement; STED, GSD, and RESOLFT with photo switchable protein. GSD microscopy uses triplet state for depleting the electron populations who can fluoresce. Since the transition lifetime of triplet state is longer than excited state, the intense laser increases the population of the electrons in the triplet state, thus depletes the population in the ground state. Therefore, the area that can fluoresce is confined at the central small area. Another approach uses photoswitchable protein under RESOFLT concept. For example, M. Hofman et al., used FP595 as photoswitchable fluorescence protein, which has ability to transit between fluorescence-activated metastable “on” state and fluorescence-inhibited metastable “off” state by the illumination of blue (on->off) and yellow (off->on) light [9].

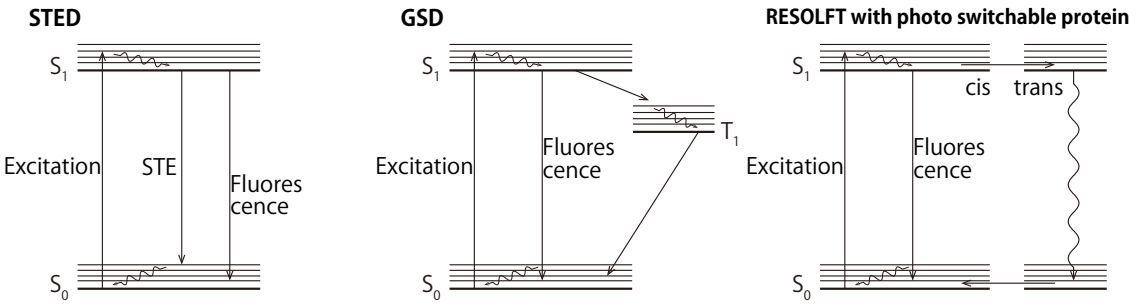

Fig. 1-6 Energy diagram of STED, GSD, and RESOLFT with photo switchable protein.

Pointillistic method for nanometer resolution imaging

Another super-resolution microscopy using non-linear optical effect is pointillistic method, such as PALM (photoactivatable localization microscopy) and STORM (stochastic optical reconstruction microscopy). PALM was also awarded Nobel Prize in 2014 together with the STED microscopy. PALM uses wide-field microscopy system, and the fluorescence probabilities of the molecules at the different position are controlled stochastically.

The pointillistic microscopy discriminates the adjacent fluorescence molecules in time dimension, and determines the position of each fluorescence molecule point by point. For example, in the case of PALM, fluorophore is designed to fluoresce when it is activated by the photoactivation laser with the wavelength different from the excitation laser for the fluorescence. First, brief photoactivation laser is illuminated to the sample so that a fraction of the fluorophores are kept in inactivated state (Fig. 1-7). The excitation laser then excites photoactivated molecules, and fluorescence image is acquired in normal wide-field fluorescence detection system. Photoactivated molecules are isolated each other by the distance distinguishable in the normal wide-field detection. Acquired images are processed to find the central position of each fluorescence molecule by fitting with PSF. Repeating this process so that all fluorophores are photobleached to determine all the coordinates of the fluorescence molecules. In principle, any photo-switchable molecule can be used for the pointillistic imaging methodology. For example, PALM uses photoactivated molecule as switching molecule, and STORM uses fluorescence molecules with the behavior of stochastic recovery from the dark state (Fig. 1-8).

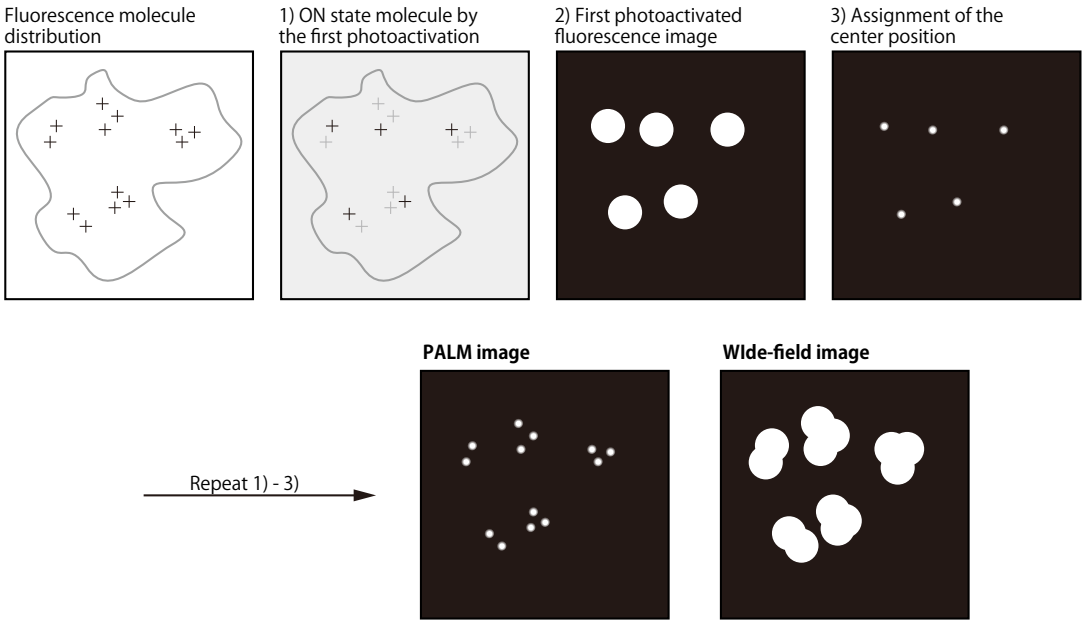

Fig. 1-7 Resolution enhancement by the photoactivated localization

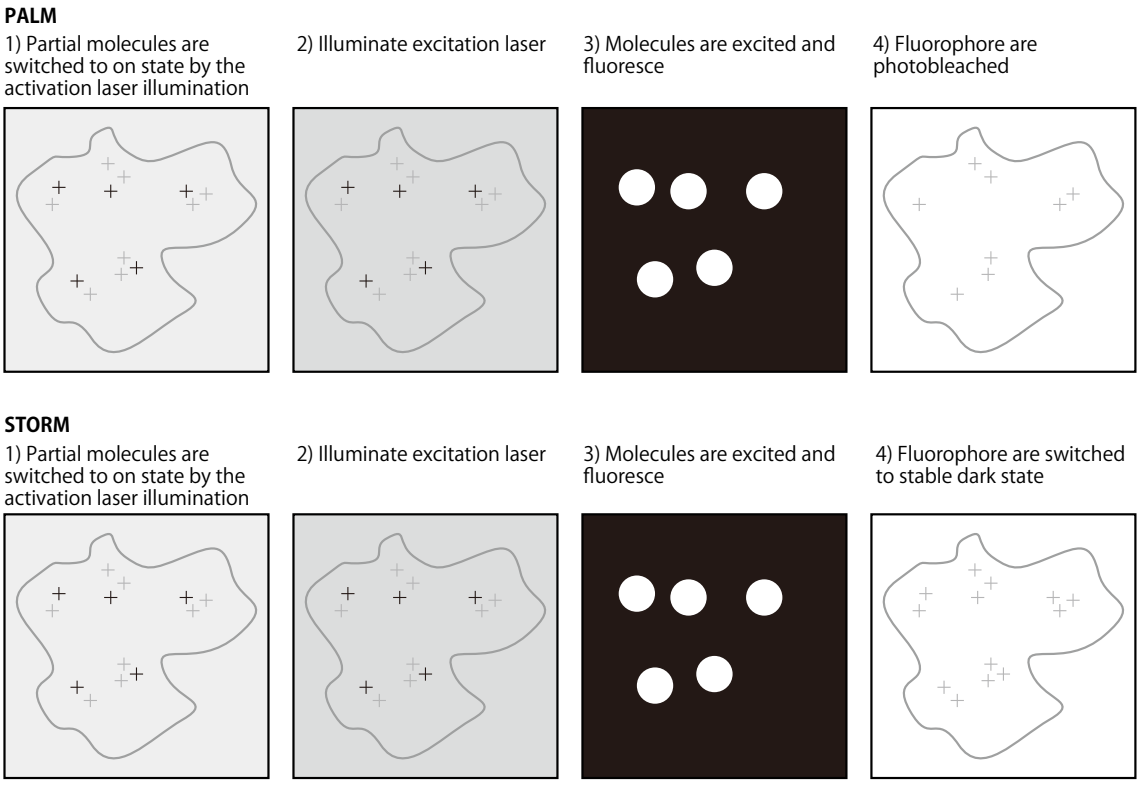

Fig. 1-8 The fluorescence on and off cycles used in PALM and STORM.

Saturable excitation for high-resolution imaging

Saturation of fluorescence can be also utilized for the resolution enhancement. SAX (saturated excitation) microscopy [10] uses confocal microscopy system and enhances the spatial resolution by extracting the saturated fluorescence from the sample. General fluorescence microscopy uses linear relationship between the excitation laser intensity to fluorescence intensity. However, if the excitation intensity is high enough, the fluorescence intensity doesn't increase linearly to the excitation intensity. This is because the population in the excited state is saturated by the effect of the finite transition lifetime and limited number of fluorescence molecules in the excited area. Extracting the saturated signal from the image, effective fluorescence area can be reduced, since the fluorescence saturation is occurred in the central part of excitation laser (Fig. 1-8).

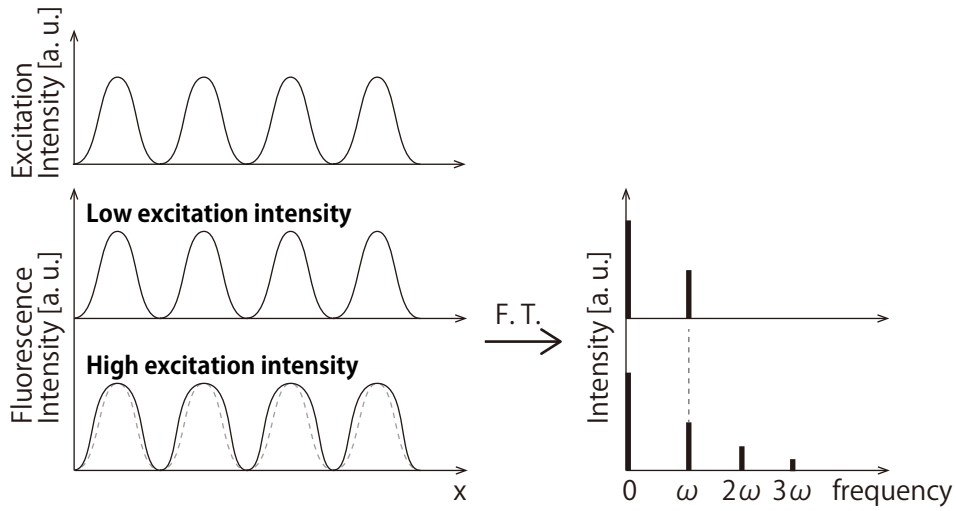

Fig. 1-8 Extraction of the higher order saturation signal decreases the effective fluorescence excitation area.

1.3 Structured illumination microscopy for wide-field high-resolution imaging

Structured illumination for resolution enhancement

Another approach to achieve high-resolution imaging utilizes the spatially structured illumination pattern to excite the fluorescence. As discussed in chapter 1.1, optical microscopy has the limitation of the spatial frequency information that can transmit through the system. SIM uses wide-field microscopy system, and illuminate the sample with spatially structured

excitation pattern instead of homogeneous excitation. As a result of the frequency mixing between illumination pattern and the sample structure, Moiré fringe pattern is appeared (Fig. 1-9). The Moiré fringe contains coarse spatial frequency information compared with the original sample structure. Therefore, the spatial frequency information, which could not transferred through conventional wide-field imaging, is transferable with structured illumination and conventional detection system. The extraction of the frequency information using the phase and the spatial frequency information of the illumination pattern enables the spatial resolution enhancement.

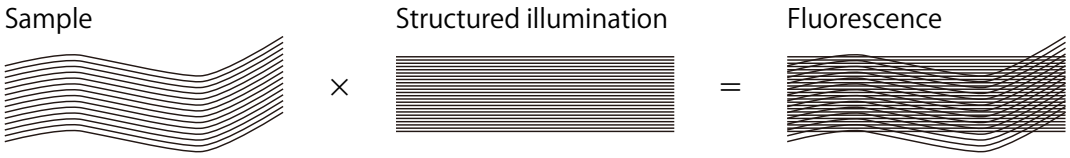

Fig. 1-9 Moiré fringe pattern is appeared as a result of the frequency mixing between the sample structure and illumination pattern.

Following arithmetic procedure carries out extraction of high frequency information[11]. Detected image D(r) can be expressed by the convolution between fluorescence from the sample and detection PSF. Fluorescence from the sample is the product of the distribution of the fluorescence molecule in the sample S(r) and illumination intensity distribution I(r), therefore, D(r) can be written as below.

$$D(r) = \big(S(r)I(r)\big) \otimes PSF(r) \tag{1-7}$$

Fourier transformation of equation 1-1 is written as

$$D(k) = (S(k) \otimes I(k))\, OTF(k) \tag{1-8}$$

If illumination pattern is sinusoidal structured pattern, I(r) can be expressed as equation 1-3.

$$I(r) = I_0\,\{1 + cos(k_1 r + \varphi)\} \tag{1-9}$$

Here, I_0, k_1, and ϕ indicate the averaged incident light intensity, spatial frequency of the illumination pattern, and illumination phase, respectively. According to equation 1-2 and 1-3, the D(k) is written as follows.

$$D(k) = I_0\,\{S(k) + 0.5\,S(k + k_1)exp(i\varphi) + 0.5\,S(k - k_1)exp(-i\varphi)\}OTF(k) \tag{1-10}$$

For simplicity, let D(K) = S(k)OTF(k), D'(k+k_1) = S(k+k_1)OTF(k), D'(k-k_1) = S(k-k_1)OTF(k). These three variables with different spatial frequency position can be separated by following arithmetic calculation.

$$\begin{pmatrix} D_1 \\ D_2 \\ D_3 \end{pmatrix} = I_0 \begin{pmatrix} 1 & 0.5\,exp(-i\varphi_1) & 0.5\,exp(i\varphi_1) \\ 1 & 0.5\,exp(-i\varphi_2) & 0.5\,exp(i\varphi_2) \\ 1 & 0.5\,exp(-i\varphi_3) & 0.5\,exp(i\varphi_3) \end{pmatrix} \begin{pmatrix} D(k) \\ D'(k+k_1) \\ D'(k-k_1) \end{pmatrix} \quad (1\text{-}11)$$

Here, D_1, D_2, D_3 are the images acquired with different illumination phase each other. Finally, resultant $D'(k+k_1)$ and $D'(k-k_1)$ are then shifted $-k_1$ and $+k_1$ to match the original position in the spatial frequency domain. Fig. 1-10 shows the schematics how the spatial frequency information As it can be illustrated in Fig. 1-10, the maximum spatial resolution enhancement is the factor of two, and the maximum detectable spatial frequency is doubled in the extended OTF.

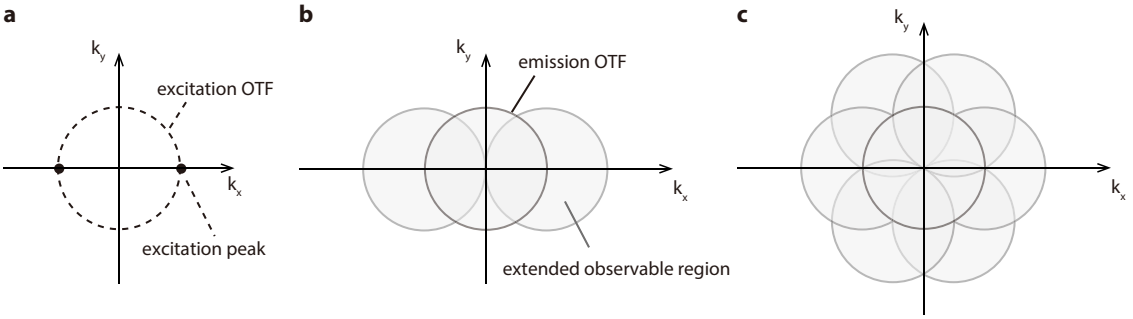

Fig. 1-10 The extraction of the spatial frequency information from the images expands the effective OTF. The maximum resolution enhancement is the factor of two in SIM.

Structured illumination with non-linear optical effect for high-speed super-resolution imaging

Super-resolution imaging utilizing the non-linear optical effect is advantageous for the few tens of nanometer level resolution. In contrast, SIM is advantageous for high-speed and relatively high-resolution imaging. Recently, there are emergent microscopy techniques that combines SIM concept with non-linear optical effect, to realize high-speed and high-resolution imaging.

M. GL. Gustafsson utilized the saturation of the fluorescence signal with SIM concept [12]. In this work, the fluorescence sample is illuminated with the spatially structured illumination pattern, and the saturated fluorescence is extracted from the detected image. Extracting the third order nonlinearity from the image, spatial resolution of fluorescence nanoparticles with the spatial resolution of sub 50 nm resolution is successfully obtained (Fig. 1-11).

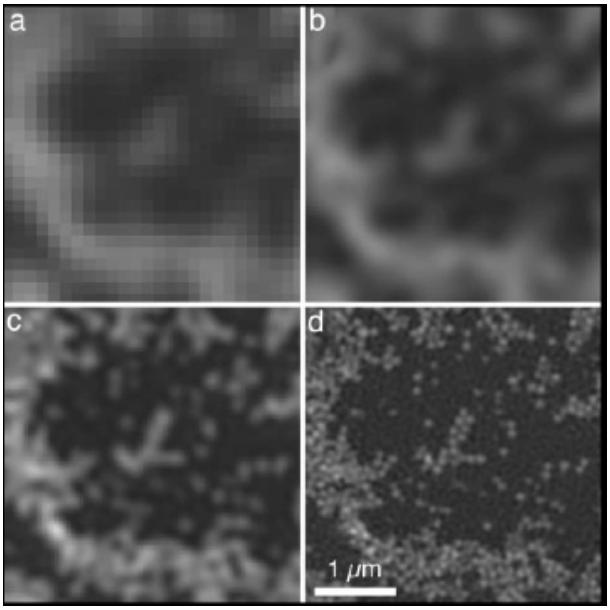

Fig. 1-11 Combination of the SIM with saturated fluorescence enabled sub 50 nm spatial resolution imaging (Images are taken from [12]). A field of 50-nm fluorescent beads, imaged by conventional microscopy (a), conventional microscopy plus filtering (b), linear structured illumination (c), and saturated structured illumination using illumination pulses with 5.3 mJ/cm^2 energy density, taking into account three harmonic orders in the processing (d).

The combination of the photoswitching molecule with SIM was reported firstly by S. Hell in 2013 [13]. This method can be understood as the parallelized illumination and the detection of RESOLFT microscopy. In that study, the live-cell imaging of the cell skeleton with the spatial resolution of 80 nm (Fig. 1-12) was successfully achieved.

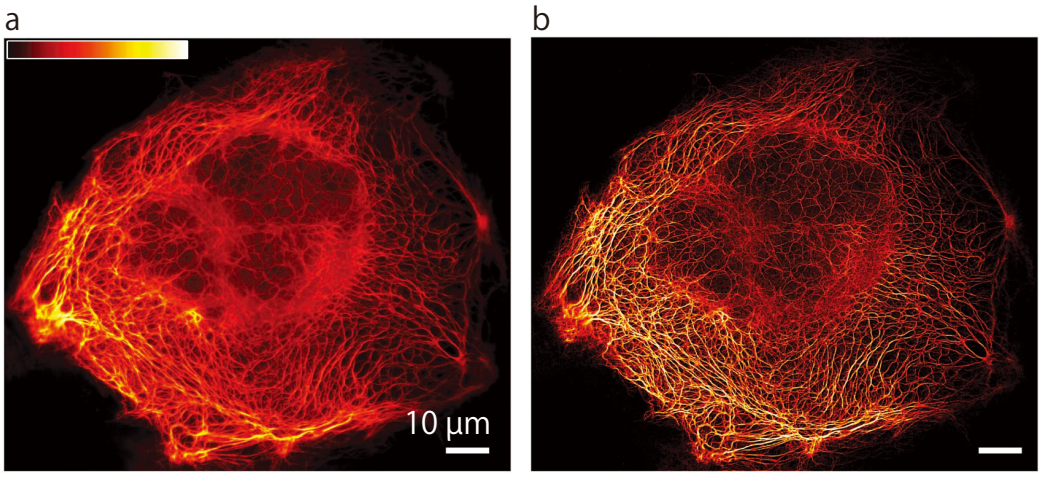

Fig. 1-12 Paralleleized RESOLFT with the concept of SIM enabled the live-cell imaging with high spatial resolution (Images are taken from [13]). The 120 μm × 100 μm field of view (wide field (a) and RESOLFT (b)) shows PtK2 cells expressing keratin 19–rsEGFP(N205S).

In 2015, E. Betzig also invented the microscopy in combination of the non-linear photoswitching effect and SIM [14]. In this study, they realized the imaging of dynamics near the living-cell's plasma membrane with the spatial resolution of 45 nm (Fig. 1-13).

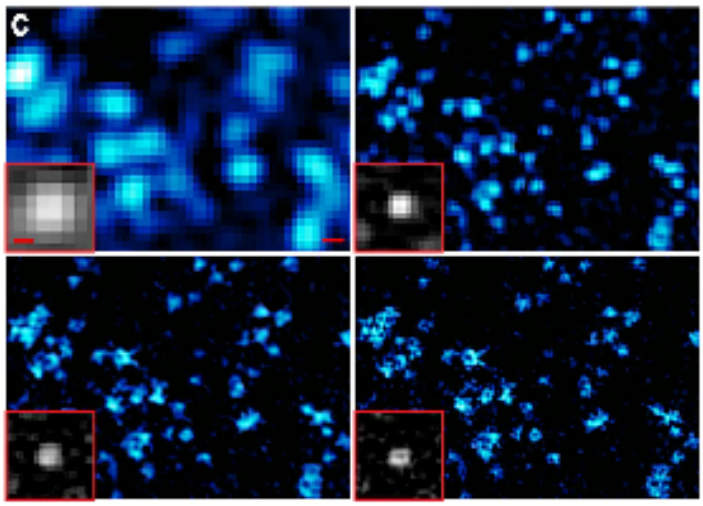

Fig. 1-13 Live-cell non-linear structured illumination microscopy based on patterned photoactivation (Images are taken from [14]). Caveolae in a COS-7 cell at 23°C transfected with Skylan-NS-caveolin was imaged with comparing TIRF with deconvolution (top left, 220-nm resolution), TIRF SIM (top right, 97-nm resolution), PA NL-SIM (bottom left, 62-nm resolution), and saturated PA NL-SIM (bottom right, 45-nm resolution). Scale bar: 200 nm. (Insets) A single caveolae pit even- tually resolved as a ring by saturated PA NL-SIM.

Optical microscopy has been played important role for the biologist to image inside the biological specimen without damaging the sample or analyzing the biological functions. Super-resolution fluorescence microscopy emerged as the powerful tool to strengthen the potential of fluorescence microscopy for nanometer resolution imaging. However, sub hundred-nanometer resolution imaging of specific samples, such as live-cell, was not realistic, because of the slow acquisition speed and high photo toxicity. Recent advances of super-resolution microscopy show the prospects of sub-hundred nanometer resolution live-cell imaging without damaging the sample. The application of the emerging super-resolution microscopy technique is now expected to contribute to study various kinds of biological dynamics.

References

[1] D. Evanko, A. Heinrichs, and C. K. Rosenthal, "Milestones in Optical Microscopy," *Nat. Milestones*, pp. 56–59,510–522, 2015.

[2] S. W. Hell and J. Wichmann, "Breaking the diffraction resolution limit stimulated-emission-depletion fluorescence microscopy by stimulated emission:," *Opt. Lett.*, vol. 19, no. 11, pp. 780–782, 1994.

[3] M. G. L. Gustafsson, "Extended resolution fluorescence microscopy Mats GL Gustafsson," *Biophys. methods*, pp. 627–634, 1999.

[4] E. Betzig, G. H. Patterson, R. Sougrat, O. W. Lindwasser, S. Olenych, J. S. Bonifacino, M. W. Davidson, J. Lippincott-Schwartz, and H. F. Hess, "Imaging intracellular fluorescent proteins at nanometer resolution.," *Science*, vol. 313, no. 5793, pp. 1642–5, Sep. 2006.

[5] M. J. Rust, M. Bates, and X. Zhuang, "Sub-diffraction-limit imaging by stochastic optical reconstruction microscopy (STORM).," *Nat. Methods*, vol. 3, no. 10, pp. 793–5, Oct. 2006.

[6] P. Wang, M. N. Slipchenko, J. Mitchell, C. Yang, E. O. Potma, and X. Xu, "Far-field imaging of non-fluorescent species with subdiffraction resolution," *Nat. Photonics*, vol. 7, no. June, pp. 449–453, 2013.

[7] S. W. Hell and M. Kroug, "Ground-state depletion fluorescence microscopy, a concept for breaking the diffraction resolution limit.," *Appl. Phys. B*, vol. 60, pp. 495–497, 1995.

[8] S. W. Hell, M. Dyba, and S. Jakobs, "Concepts for nanoscale resolution in fluorescence microscopy.," *Curr. Opin. Neurobiol.*, vol. 14, no. 5, pp. 599–609, Oct. 2004.

[9] M. Hofmann, C. Eggeling, S. Jakobs, and S. W. Hell, "Breaking the diffraction barrier in fluorescence microscopy at low light intensities by using reversibly photoswitchable proteins," *PNAS*, vol. 595, no. 11, 2005.

[10] K. Fujita, M. Kobayashi, S. Kawano, M. Yamanaka, and S. Kawata, "High-Resolution Confocal Microscopy by Saturated Excitation of Fluorescence," *Phys. Rev. Lett.*, vol. 99, no. 22, p. 228105, Nov. 2007.

[11] B.-J. Chang, L.-J. Chou, Y.-C. Chang, and S.-Y. Chiang, "Isotropic image in structured illumination microscopy patterned with a spatial light modulator.," *Opt. Express*, vol. 17, no. 17, pp. 14710–21, Aug. 2009.

[12] M. G. L. Gustafsson, "Nonlinear structured-illumination microscopy: wide-field fluorescence imaging with theoretically unlimited resolution.," *Proc. Natl. Acad. Sci. U.*

S. A., vol. 102, no. 37, pp. 13081–6, Sep. 2005.

[13] A. Chmyrov, J. Keller, T. Grotjohann, M. Ratz, E. D'Este, S. Jakobs, C. Eggeling, and S. W. Hell, "Nanoscopy with more than 100,000 'doughnuts,'" *Nat. Methods*, no. July, Jul. 2013.

[14] D. Li, L. Shao, B. Chen, X. Zhang, M. Zhang, B. Moses, D. E. Milkie, J. R. Beach, J. a H. Iii, M. Pasham, T. Kirchhausen, M. a Baird, M. W. Davidson, P. Xu, and E. Betzig, "Extended-resolution structured illumination imaging of endocytic and cytoskeletal dynamics," *Science*, vol. 349, no. 6251, p. aab3500, 2015.

Chapter 2
Line illumination for structured illumination microscopy

In this chapter, the application of SIM to line illumination microscopy is discussed. Line illumination microscopy with slit-detection enables the optical-sectioning imaging with higher acquisition speed than point illumination. In addition, line illumination can be combined with optics for spectroscopy, which realizes the high-resolution spectral imaging by using structured illumination. As the first part of chapter 2, I introduce a spectral imaging method using line illumination. For the latter part of this chapter, the imaging characteristic of the structured line illumination microscopy for hyperspectral imaging with high spatial resolution is discussed.

2.1 Spectral imaging capability with structured line illumination microscopy (SLIM)

Application of the SIM to line illumination microscopy has the potential for the high-spatial resolution spectral imaging. Spectral imaging, such as Raman imaging [1] or hyper spectral fluorescence imaging [2][3], requires obtaining spectral information at each spatial position. Therefore, the obtained dataset contains three-dimensional information for each image plane, x, y, and spectral dimension. Detecting the three-dimensional dataset using two-dimensional image detector is possible by either scanning the detection point or using two dimensional spectral fiber arrays. Fig. 2-1 shows an example of the optical setup of spectral imaging using spectrometer for the detection. The incident laser is illuminated to the point on the sample, and the focus is scanned in x-y direction. Spectral signal from each sample position is corrected through the dichroic filter, and spectrum is detected by spectrometer.

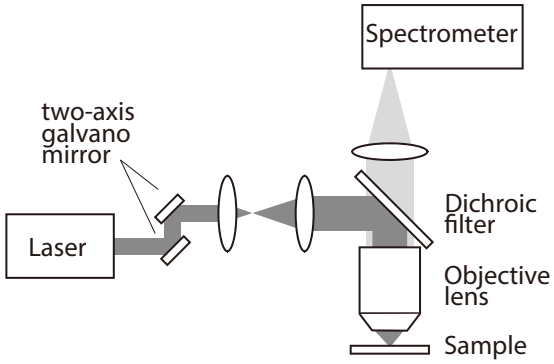

Fig. 2-1 Optical setup for point scanning spectral imaging using spectrometer for detection.

Line illumination can be used for the spectral imaging as well as point illumination system by combining a 2D detector. Since the line illumination enables parallel detection of signal light from multiple points in a sample, the imaging speed can be greatly shortened compared to that with point scanning. This is especially useful for hyperspectral imaging with weak signals, such as Raman microscopy. K. A. Christensen et al., has implemented line illumination into Raman microscopy with the use of a Powell lens in 1998 [4]. In this study, they illuminate the sample with line-shaped illumination using Powell lens and detect Raman scattering from the sample with slit-spectrometer. With the use of line illumination, they succeeded to achieve 100 spectra at the same time. Hamada et al has reported the imaging of dynamics of living cells with high NA objective lens of 1.27 and large area detector [5]. In this study, they illuminate the sample with line-shaped illumination and detect with slit-spectrometer (Fig. 2-2). The imaging speed of this study is 400 times shorter than the point-scanning case.

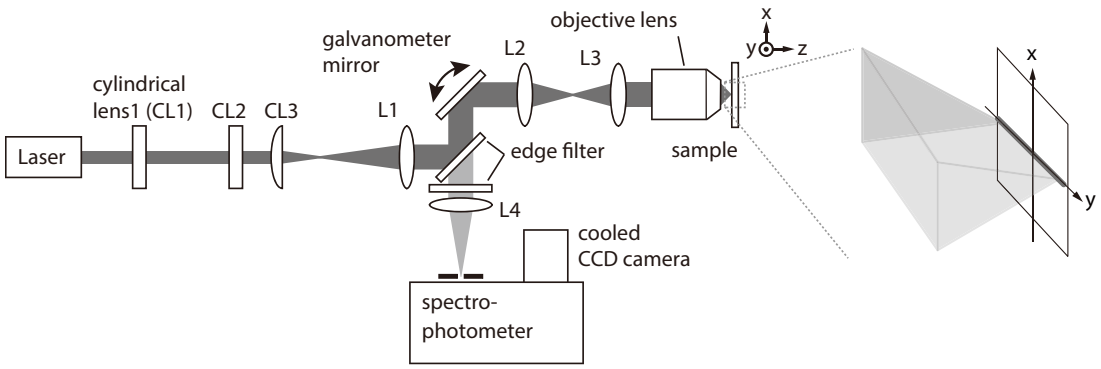

Fig. 2-2 Optical system of line-illumination Raman microscopy

The application of SIM to slit-confocal microscopy has an advantage in observation

of thick samples. Conventional SIM is equipped with wide-field fluorescence microscopy; therefore, the imaging of thick fluorescent samples with SIM has been difficult. The out-of-focus signal degrades the contrast of the structured pattern information in a image, therefore the resultant image contains the image artifact [6]. In the fluorescence SIM, it has been reported that the use of line illumination in SIM can suppress the signal from out-of-focus. Since the slit detection realizes optical sectioning similar to that in confocal detection, artifacts originated from the out-of-focus contribution are effectively suppressed (Fig.2-3).

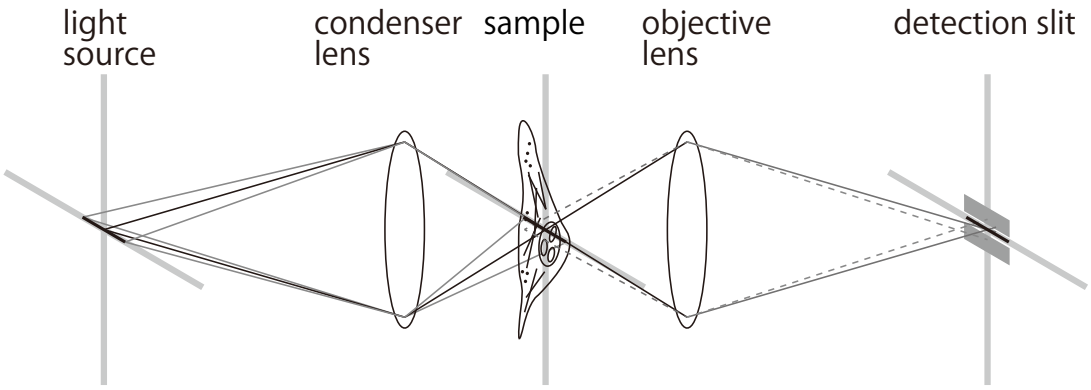

Fig. 2-3 Schematics of the slit-confocal microscopy. The detection slit effectively removes the out-of-focus light in the direction parallel to the slit.

2.2 Imaging property of SLIM

Apparatus in SLIM imaging

SLIM using a slit detector provides a different imaging property, comparing with the conventional wide-field SIM. As discussed in Chapter 1, SIM can enhance the spatial resolution in the direction perpendicular to the illuminated grid pattern by a factor of two at the maximum. To realize a SLIM system, there are two possible optical design considering the trade-off between imaging speed and resolution enhancement: 1) To use the full potential of the spatial resolution enhancement ~2x in grid direction, and rotate the illumination pattern to achieve the homogeneous resolution enhancement in lateral direction, 2) To use coarse illumination pattern to enhance the spatial resolution ~1.4x to balance the resolution enhancement in slit direction. In the case 1, the acquisition speed is 3 to 5 times longer than the case 2, however, the resolution improvement in lateral direction is high. In the case 2, it has advantage for the fast image acquisition and axial resolution, but the achievable resolution enhancement in lateral resolution is limited. Moreover, there is a trade-off between lateral and axial resolution improvement. This is because the focusing effect in the direction perpendicular to the illumination line is stronger when the illumination beam goes through near the center of the objective pupil, where the resolution enhancement by SIM is small. In chapter 2.2, the imaging property in SLIM and the trade-off between lateral and axial resolution are discussed.

For the SLIM experiment, we can choose either two-beam or three-beam interference system. Three-beam interference system enables three-dimensional resolution improvement. However, higher signal-to-noise ratio is required for the image reconstruction, since we have to extract information from 5 different orders to reconstruct the three-dimensional spatial frequency information. An example of optical setup for SLIM using two-beam interference is shown in Fig. 2-4. The grating is inserted at the position, which is optically conjugate to the imaging plane, and the beam stop is placed at the reciprocal plane to cut the unwanted diffraction order beam. Field rotator in this setup is used to rotate the illumination pattern so that the homogeneous resolution improvement is obtained in all lateral direction. In order to improve the resolution in the direction perpendicular to the illumination line, acquired images can be processed as described in the reference [6]. Another possibility is to insert physical slit before the image detector, and use stage scanning instead of laser scanning, if the rotation of the illumination is necessary. If the rotation of the illumination is not required, it is possible to choose the illumination scanning using one-axis galvanometer mirror, which is placed at the

position that can de-scan the fluorescence from the sample as well.

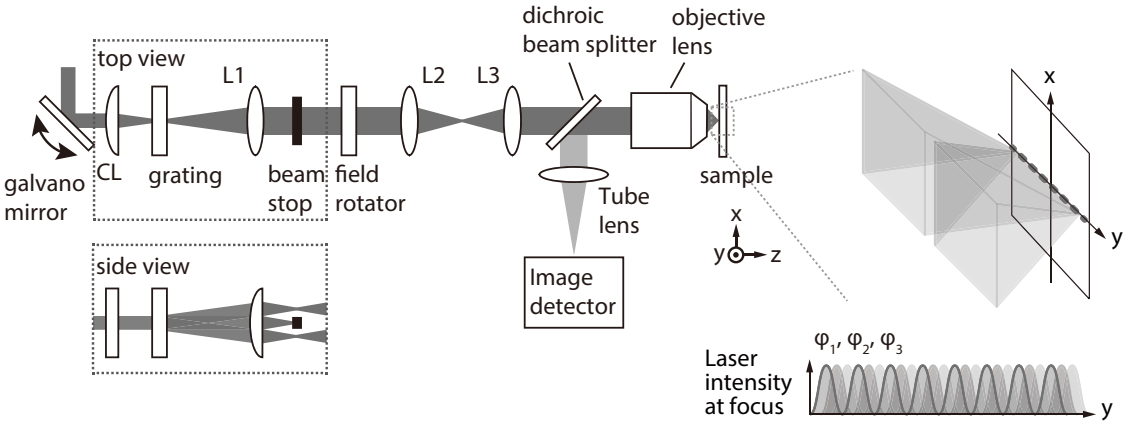

Fig. 2-4 Optical setup of SLIM. Structured line illumination pattern, which is formed by the interference of the beam, illuminates the sample. CL: cylindrical lens.

Image formation in SLIM

In the image formation of the SLIM, illumination line length at the objective pupil affects on the both lateral and axial resolution [7]. The illumination PSF can be calculated by the Fourier transformation of the pupil function of the objective lens, which is used for the illumination of the sample. Fig. 2-5 shows the schematics of the pupil function in SLIM. In the case of two-beam interference, two lines are focused at the pupil of the objective lens by the L3 in Fig. 2-4. Therefore, the illumination pupil function can be calculated by the multiplication of the focused lines with objective aperture function. For the simplicity, I consider the profile of the focused lines as the Gaussian function centered at $x = \pm x_m$, and the intensity distribution in y-axis is homogeneous. The line at the pupil is written as the convolution of the focused line Fl with two delta functions.

$$u_a(x_a, y_a) = P(x_a,\ y_a)\{Fl(x_a) \otimes (\delta(x_a + x_m) + \delta(x_a - x_m))\} \qquad (2\text{-}1)$$

Here, P (x_a, y_a) is the aperture function of objective lens.

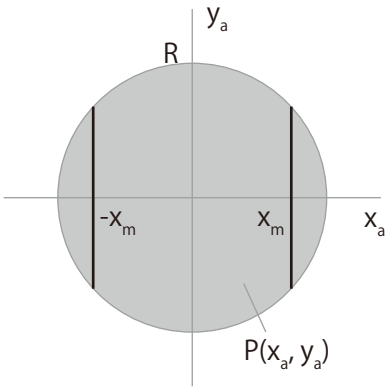

Fig. 2-5 Pupil function for the illumination in SLIM.

As it can be seen in the Fig. 2-5, the increase of the x_m will decrease the length of the line at the pupil, which results in weaken the focusing at the sample, thus the axial resolution is expected to degrade. In contrast, the resolution enhancement in x-direction is increased as x_m increases as indicated in chapter 1. For the discussion of the lateral resolution and axial resolution in SLIM, we can consider the effective pupil function, P_{eff}, as indicated in Fig. 2-6.

$$u_a(x_a, y_a) = P_{eff}(x_a, y_a;\, x_m)\{Fl(x_a) \otimes (\delta(x_a + x_m, y_a) + \delta(x_a - x_m, y_a))\} \qquad (2\text{-}2)$$

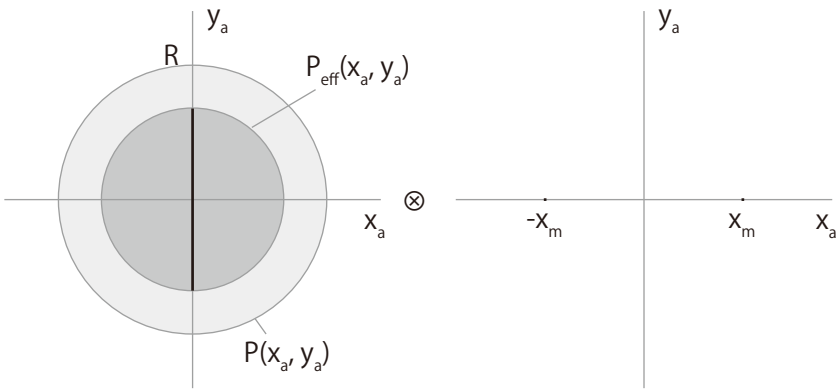

Fig. 2-6 The pupil function can be described by the convolution of the line focusing with two delta functions.

The amplitude distribution of the focused illumination pattern u_f can be calculated by the three dimensional Fourier transformation of the equation 2-2.

$$\begin{aligned} u_f(x_f, y_f, z_f) &= L_{effill}(y_f, z_f) \times FT(\delta(x_a + x_m) + \delta(x_a - x_m)) \\ &= L_{effill}(y_f, z_f) \times \cos\left(\frac{1}{2} w_m x_f + \phi\right) \end{aligned} \qquad (2\text{-}3)$$

Here, L_{effill} is the amplitude intensity of line-shaped focused beam with the pupil function of P_{eff},

which has homogeneous amplitude distribution in x. The intensity distribution of the illumination pattern is

$$I_f(x_f, y_f, z_f) = \left|L_{effill}(y_f, z_f)\right|^2 \times \frac{1}{2}\{1 + \cos(w_m x_f + \phi)\}$$
$$= PSF_{ill} \times \frac{1}{2}\{1 + \cos(w_m x_f + \phi)\} \quad (2\text{-}4)$$

It is know that in the confocal microscopy with finite sized detection pinhole, detection PSF is written as below, with the spatial function of pinhole d, which is written in the unit equivalent to sample plane unit [8]. The effective detection PSF is the three-dimensional convolution between the function of the detector and the intensity PSF of the incoherent imaging.

$$PSF_{det} = PSF(r) \otimes d(r) \quad (2\text{-}5)$$

$$d(x, y, z) = \begin{cases} 1 & : (x^2 + y^2)^{1/2} \leq a, z = 0 \\ 0 & : otherwise \end{cases} \quad (2\text{-}6)$$

Here, a is the radius of the pinhole placed in front of the detector. In the case of slit detector, whose width of b placed at the position of y = 0, the detector function of the slit can be rewritten as below.

$$d(x, y, z) = \begin{cases} 1 & : |x| \leq \frac{b}{2}, y = 0, z = 0 \\ 0 & : otherwise \end{cases} \quad (2\text{-}7)$$

The detection PSF in slit-scanning microscopy is obtained by the two-dimensional convolution in x- and z-axis of the detector function with the intensity PSF of incoherent imaging.

Image formation in SLIM can be therefore treated by modifying OTF in the wide-field SIM to effective OTF [9]. The image formation in incoherent imaging can be described by the three dimensional convolution between effective PSF and distribution of the sample D(r).

$$D(r) = S(r) \otimes PSF_{eff}(r) \quad (2\text{-}8)$$

For the SLIM,

$$PSF_{eff} = \left[PSF_{ill} \times \frac{1}{2}\{1 + \cos(w_m x_f + \phi)\}\right] \times PSF_{det} \quad (2\text{-}9)$$

Calculation results

The effective OTF is calculated by vectorial theory [10][11] using the software that is developed by Prof. Heintzmann's group in Institute of photonics technology (biological nanoimaging research group, IPHT, Germany). The effective OTF is calculated by the Fourier transformation of effective PSF. Comparing with traditional calculation method which treats

scalar theory [12], vectorial calculation is advantageous to calculate 3D OTF with arbitral aberrations, pupil functions or asymmetric polarized light such as linearly polarized light, with the expense of calculation cost. The amplitude of the focused light at the focal plane of the objective lens are calculated by the Fourier transformation of the pupil function prepared by the two dimensional projection of the masked three dimensional Ewalt sphere, taking account for the polarization and pupil mask [10]. In order to calculate the focused pattern at the focal plane, the two lines, which have Gaussian profile in y-axis and homogeneous intensity distribution in x-axis, mask the pupil plane of the objective lens. The linear polarization in the perpendicular to the line at the focal plane is assumed.

Here, we compared the profile of the effective OTF in the each system. The depth resolution and x-resolution is compared by making the profile of the OTF for each x_m value. For the simplicity, I define the aperture ratio Ar as below.

$$Ar = {}^{x_m}\!/_{R} \tag{2-10}$$

Left figure of Fig. 2-7 shows the one example of the objective pupil for the calculation. The position of the two lines are separated for $2x_m$. The square root of the three dimensional Fourier transformation of pupil function make the intensity distribution of the illumination pattern. Structured line illumination used in this study is shown as right figure of Fig. 2-7.

Fig. 2-7 The intensity distribution of the incident beam at the objective pupil (left) and sample plane (right).

The effective OTF in SLIM is calculated by the equation (2-9). In this calculation, the PSF_{illu} is calculated by the Fourier transformation of the line at the objective pupil with the

effective line length. Then PSF_{total} is obtained by the multiplication of PSF_{illu} with PSF_{det} of the system. OTF_{total} is calculated by the Fourier transformation of OTF_{total}, and then shifted for the k, which is the frequency of the illumination pattern. The detection PSF is calculated assuming the detection slit width of 1 Airy unit, and the illumination pattern direction is kept in the same direction.

Fig. 2-8 shows the profile of the effective OTF in y- and z- axis with different Ar. As it can be seen from the log intensity plot, spatial resolution in y-axis is improved as the increase of Ar. In contrast, spatial resolution in x-axis and z-axis is decreased as the increase of Ar, since the focusing of the illumination pattern is worse with the line length at the objective pupil shorten.

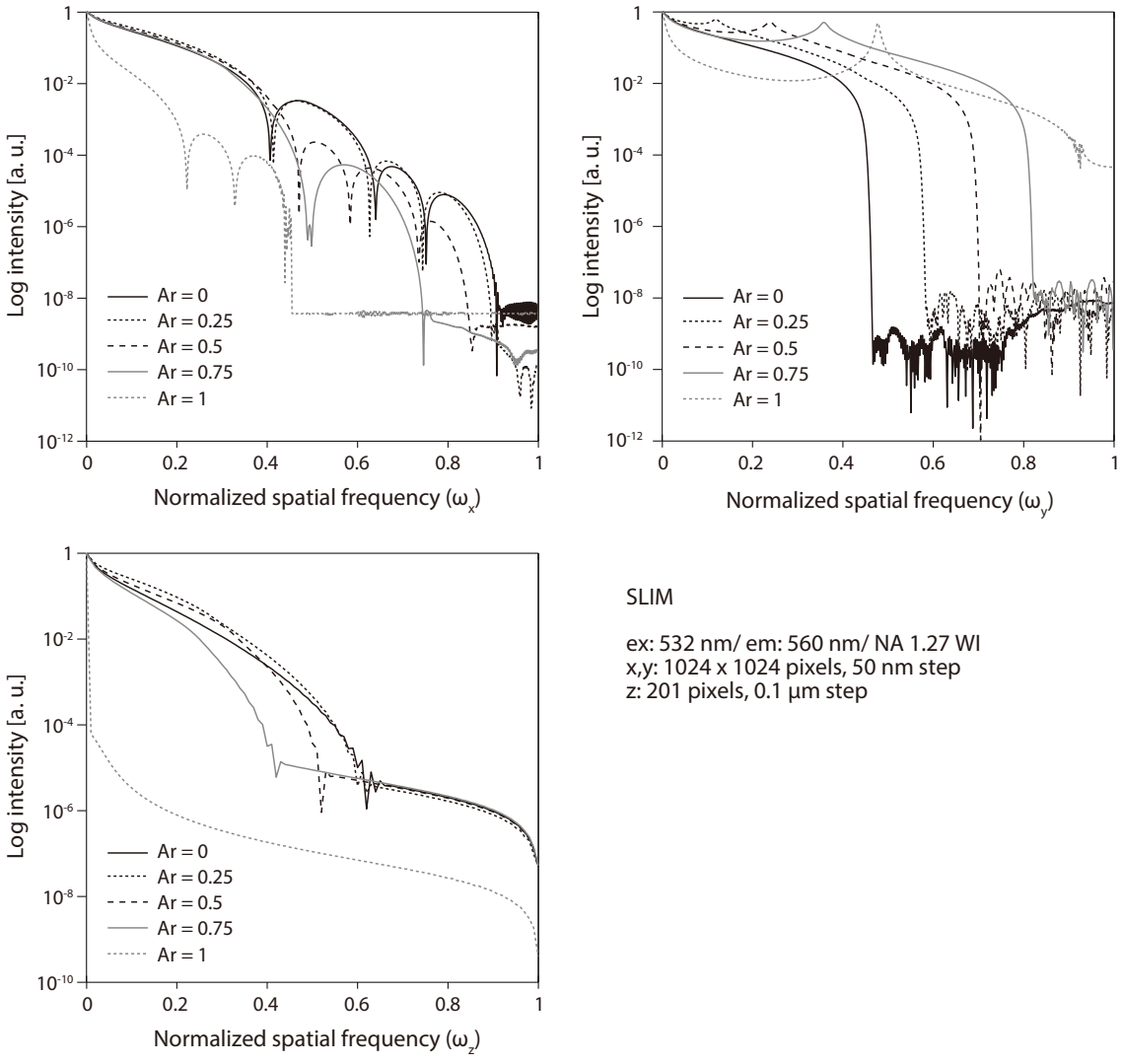

Fig. 2-8 Comparison of the profile of effective OTF with different Ar.

Fig. 2-9 shows the comparison of the profiles of effective PSF with different Ar. It can be clearly seen that the width of the x- and z-profiles of PSF become wider as Ar increased, in contrast, the y-profile of PSF become narrower as Ar increased. It should be note that the resultant PSF shows the ringing side-lobe, which may arise the image artifact. This side-lobe can be result from the peak in the effective OTF that can be seen in Fig. 2-8. For the actual application of the SIM, the shape of the OTF is compensated in a way, which is indicated in the literature [13][14], however, in this section, the OTF is not compensated to show the effect of the different Ar value.

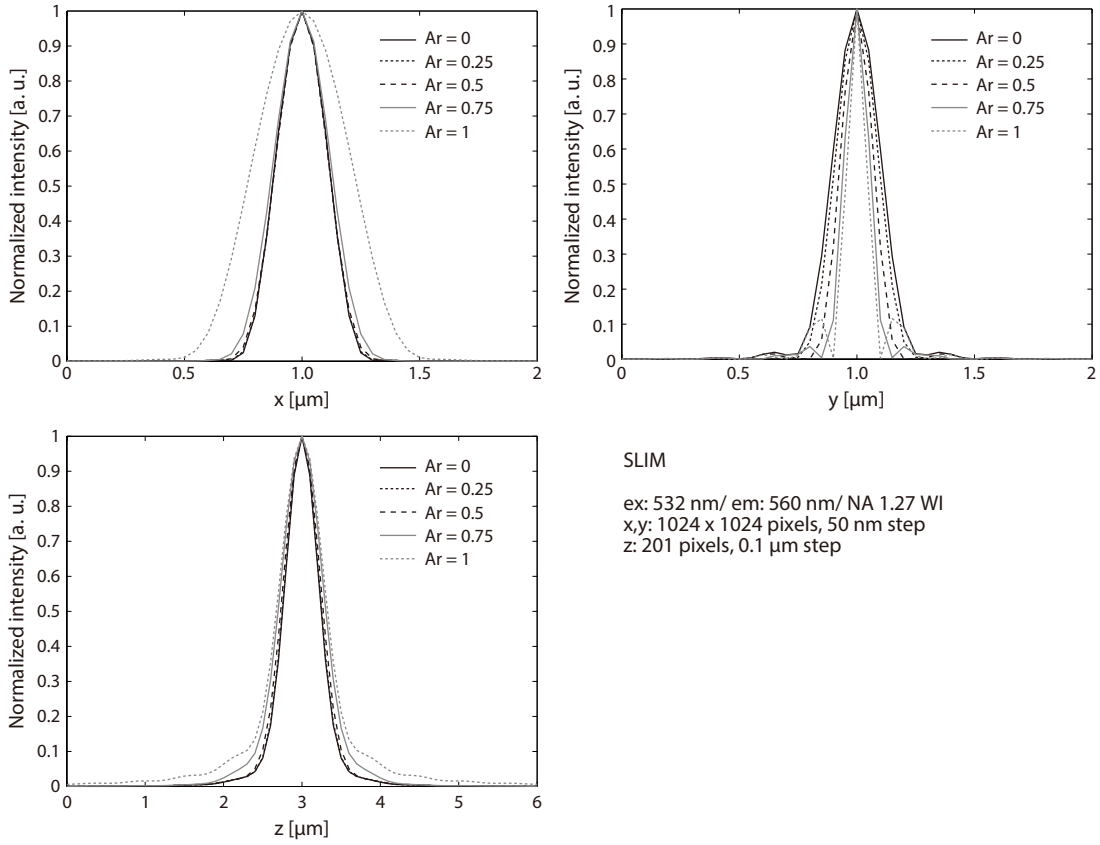

Fig. 2-9 x, y, z-profiles of effective PSF with different Ar value.

Fig.2-10 shows the comparison of FWHM value with different Ar. The FWHM value is normalized by the maximum value in the data set for comparison. From the figures, it is seen that the x- and z-resolution is changed after the Ar of 0.75. As a result of the trade-off between the x-, z-resolution and y-resolution, the Ar of ~0.75 is considered as the practical choice for the SLIM [6][7]. In the evaluation of the OTF, I set the detection slit width of a Airy unit, not the

infinitely small slit width, which was used in the reference [7]. Also, I compared the x-resolution, so that the evaluation of the different optical design can be possible.

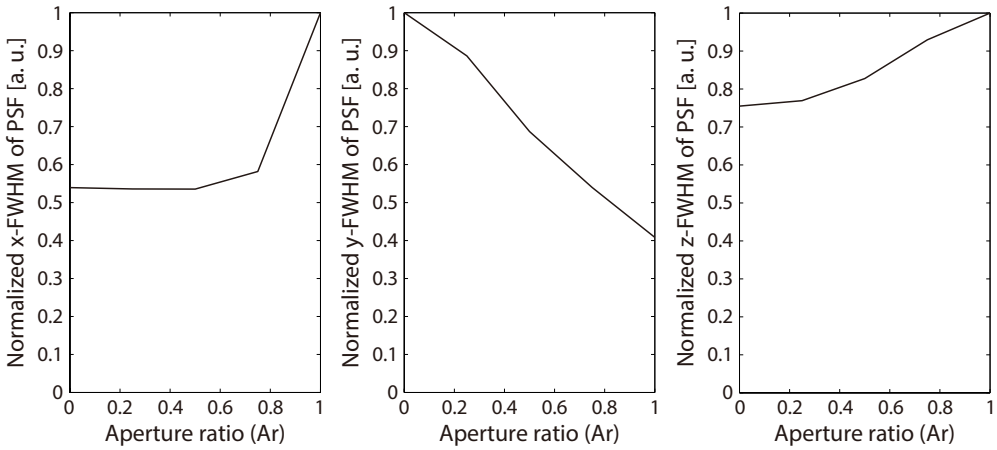

Fig. 2-10 Comparison of the FWHM of PSF with different Ar.

Discussion

As described in chapter 2-1, we can consider possible two optical design of SLIM. If one wants to increase the spatial resolution in x, it is desirable to use higher Ar, however, the effect of the suppression of out-of-focus light is not very high. Therefore, Ar of 0.75 is generally can be used for this system as described above. Different possibility of the setup is using the Ar of 0.5, which ensures the y-resolution enhancement for ~1.4x, to obtain the resolution enhancement as confocal microscope. This optical design prevents the resolution degradation in x-axis by the effect of increased Ar value, which can be seen in Fig. 2-10. Such setup is effective for the detection, which requires long integration time, such as spontaneous Raman scattering detection. Shorter total image integration time can be achieved because this setup doesn't require the rotation of the illumination pattern.

References

[1] A. F. Palonpon, J. Ando, H. Yamakoshi, K. Dodo, M. Sodeoka, S. Kawata, and K. Fujita, "Raman and SERS microscopy for molecular imaging of live cells," *Nat. Protoc.*, vol. 8, no. 4, pp. 677–692, Mar. 2013.

[2] M. J. Booth, a Jesacher, R. Juskaitis, and T. Wilson, "Full spectrum filterless fluorescence microscopy.," *J. Microsc.*, vol. 237, no. 1, pp. 103–9, Jan. 2010.

[3] L. Gao, N. Hagen, and T. S. Tkaczyk, "Quantitative comparison between full-spectrum and filter-based imaging in hyperspectral fluorescence microscopy.," *J. Microsc.*, vol. 246, no. 2, pp. 113–23, May 2012.

[4] K. A. Christensen and M. I. D. Morris, "Hyperspectral Raman Microscopic Imaging Using Powell Lens Line Illumination," *Appl. Spectrosc.*, vol. 52, no. 9, pp. 1145–1147, 1998.

[5] K. Hamada, K. Fujita, N. I. Smith, M. Kobayashi, Y. Inouye, and S. Kawata, "Raman microscopy for dynamic molecular imaging of living cells," *J. Biomed. Opt.*, vol. 13, no. August 2008, pp. 1–4, 2008.

[6] O. Mandula, M. Kielhorn, K. Wicker, G. Krampert, I. Kleppe, and R. Heintzmann, "Line scan--structured illumination microscopy super-resolution imaging in thick fluorescent samples.," *Opt. Express*, vol. 20, no. 22, pp. 24167–74, Oct. 2012.

[7] T. Kim, D. Gweon, and J.-H. Lee, "Enhancement of fluorescence confocal scanning microscopy lateral resolution by use of structured illumination," *Meas. Sci. Technol.*, vol. 20, no. 5, p. 055501, May 2009.

[8] S. Kawata, R. Arimoto, and O. Nakamura†, "Three-dimensional optical-transfer-function analysis for a laser-scan fluorescence microscope with an extended detector," *J. Opt. Soc. Am. A*, vol. 8, no. 1, p. 171, Jan. 1991.

[9] D. Li, L. Shao, B. Chen, X. Zhang, M. Zhang, B. Moses, D. E. Milkie, J. R. Beach, J. a H. Iii, M. Pasham, T. Kirchhausen, M. a Baird, M. W. Davidson, P. Xu, and E. Betzig, "Extended-resolution structured illumination imaging of endocytic and cytoskeletal dynamics," *Science*, vol. 349, no. 6251, p. aab3500, 2015.

[10] M. R. Arnison and C. J. R. Sheppard, "A 3D vectorial optical transfer function suitable for arbitrary pupil functions," *Opt. Commun.*, vol. 211, no. October 2002, pp. 53–63, 2006.

[11] B. R. Frieden, "Optical Transfer of the Three-Dimensional Object * t," *J. Opt. Soc. Am.*, vol. 57, no. I, p. 56, 1967.

[12] C. J. R. Sheppard, M. Gu, Y. Kawata, and S. Kawata, “Three-dimensional transfer functions for high- aperture systems,” *J. Opt. Soc. Am. A*, vol. 11, no. 2, p. 593, 1994.

[13] M. G. L. Gustafsson, “Extended resolution fluorescence microscopy Mats GL Gustafsson,” *Biophys. methods*, pp. 627–634, 1999.

[14] M. G. L. Gustafsson, L. Shao, P. M. Carlton, C. J. R. Wang, I. N. Golubovskaya, W. Z. Cande, D. a Agard, and J. W. Sedat, “Three-dimensional resolution doubling in wide-field fluorescence microscopy by structured illumination.,” *Biophys. J.*, vol. 94, no. 12, pp. 4957–70, Jun. 2008.

Chapter 3
Application of SLIM to Raman imaging

Raman microscopy is a powerful tool for analyzing the rich chemical information of the specimen from the spectrum. However, the spatial resolution of Raman microscopy has been still limited to the range of the diffraction limit. In this chapter, I describe the application of the SLIM for resolution improvement in Raman microscopy. After brief introduction of Raman scattering and Raman microscopy, the implementation of SLI to Raman microscopy and the imaging property of the microscope are described with the experimental results of imaging samples for system evaluation and practical applications.

3.1 Raman microscopy as analytical imaging

Raman scattering

The first physical explanation of the Raman scattering has been given by C. V. Raman on 1928 [1]. He observed the wavelength shift of the scattered light compared to the incident wavelength, using sunlight as a light source and his eyes as detector. It was later named Raman effect, and he was awarded the Nobel Prize two years after the publication of Raman effect [2]. Since the wavelength shift corresponds to the molecular vibrational energy of the specimen, one can obtain rich molecular information, such as species, amount, temperature and environment around the molecule, from the Raman spectrum. Therefore, Raman spectroscopy has been considered as a powerful tool for analyzing varieties of materials. Owing to the advancement of high-power lasers and high-sensitivity detectors, Raman microscopy is now grown to the standard method to analyze various kinds of specimen: such as carbon materials, biological tissues, and medicines.

Raman scattering can be understood as inelastic light scattering between photons and a material. When the light is irradiated to a sample, a portion of scattered light shows wavelength shift compared to that of the incident light. The scattering with wavelength shift of Ω_R is called Raman scattering, and Ω_R is called Raman shift. Assuming the frequency of the incident light is ω_1, scattered light with the frequency of ω_1, $\omega_1 - \Omega_R$, and $\omega_1 - \Omega_R$ are defined as

Rayleigh scattering, Stokes scattering, and anti-Stokes scattering, respectively (Fig. 3-1). This is because the partial energy of the photon transferred to the molecular vibration energy as a result of the interaction between photon and molecules. Ω_R corresponds to the energy of the molecular vibration in the sample. Therefore, by detecting the Raman spectrum and comparing it to the reference Raman spectra, we can specify which molecule is in the sample. In addition, it is also possible to analyze the state of the specimen since the environment or the temperature around the molecule can affect the molecular vibrational state.

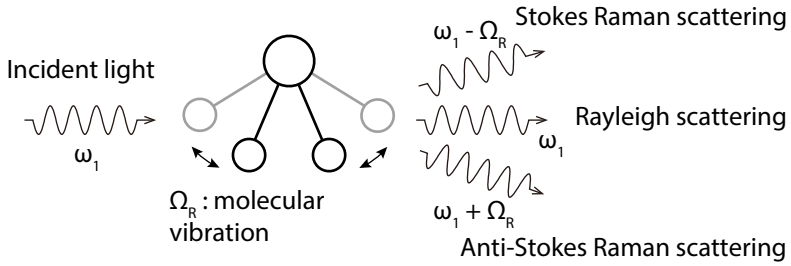

Fig. 3-1 The wavelength shift of Raman scattering is originated from vibrational excitation.

Fig. 3-2 shows the example of the Raman spectra obtained from a living HeLa cell [3]. As it can be seen from the figure, one Raman spectrum contains much information from the different vibrational states of intracellular molecules.

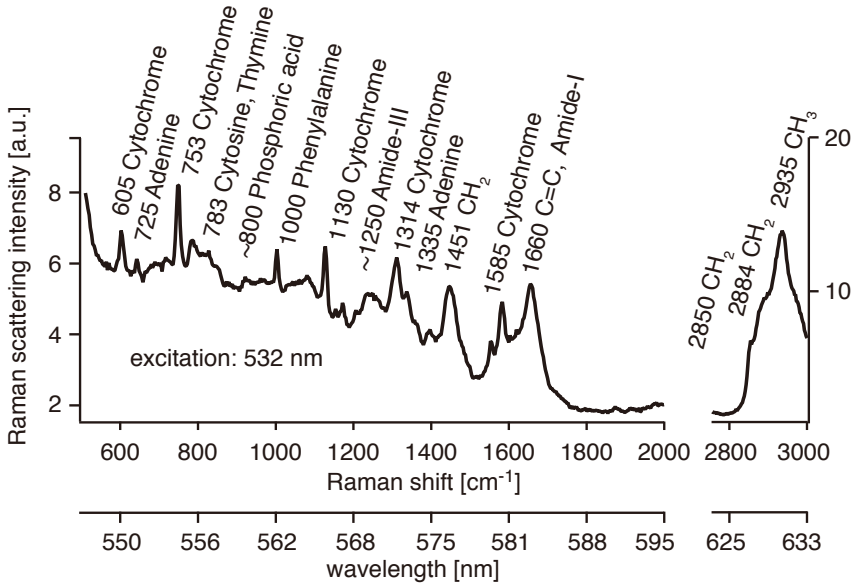

Fig. 3-2 Raman spectra obtained from the living HeLa cell [3][4] (Raman spectrum is taken from [3]).

Raman spectroscopy to Raman microscopy

In 1980s, it was realized to use Raman scattering for the imaging of the sample, not only for the spectroscopy. The invention of the high-power laser and the high-sensitivity multichannel detector enabled micro-spectroscopy in the reasonable time scale. Raman microscopy is equipped with spectrometer for high-sensitivity imaging or interferometer based Fourier transformation system for high-spectral resolution imaging. For the both cases, it requires scanning of the illumination. As introduced in Chapter 2.1, point-scanning and slit-scanning microscope can be used for the spectral Raman imaging. Fig. 3-3 shows how a Raman image is constructed. Raman spectra are measured at the different sample positions, and a three-dimensional Raman dataset is obtained. Plotting spatial distribution of Raman scattering intensity at a specific wavenumber, we can obtain an image showing the distribution of molecular vibrations.

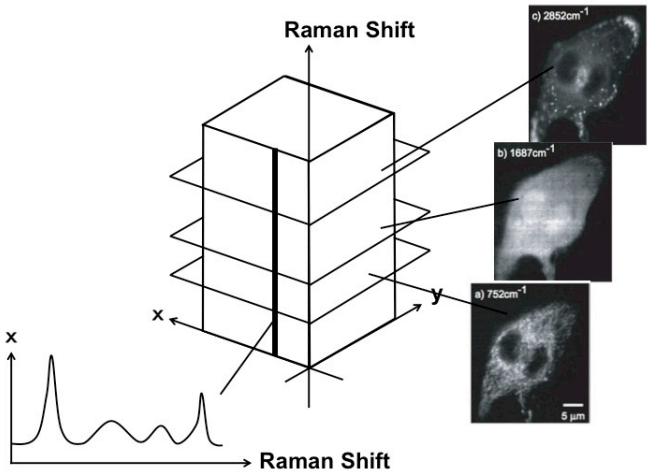

Fig. 3-3 Reconstruction of Raman scattering intensities at the different sample positions shows the spatial distribution of specific molecular vibrations.

3.2 Development of SLI Raman microscope

Optical setup of SLI Raman microscope

Although the Raman microscopy is the powerful tool for the imaging and analysis of various kinds of the specimen, the spatial resolution of Raman microscope has been limited to the classical diffraction limit. In this study, I developed a high-spatial-resolution Raman microscope with the spatial resolution below the diffraction limit, by combining structured illumination with slit-confocal Raman microscope. The results and images shown here has been partially published in [5].

I developed the optical system shown in Fig. 3-4. As discussed in Chapter 2.2, there are two possible optical designs in SLI Raman microscopy, considering the trade-off between acquisition time and the resolution enhancement. In this study, I designed the optics with the aperture ratio (Ar) of ~0.5 to realize the balanced resolution enhancement in lateral direction, with a reasonable acquisition time scale. In order to shape the illumination in line with strong focusing in the direction perpendicular to the line illumination, three cylindrical lens set is used: first two cylindrical lenses expand the laser in one axis, and the last cylindrical lens focus the line in another axis. One-axis galvanometer mirror is used to scan the line in x at the sample plane. As a result of the interference between ±1st order diffraction light, line illumination with a fringe pattern in y-axis is created. Raman scattering from the illuminated area is detected by a cooled-CCD camera equipped in an imaging spectrophotometer through two long-pass edge filters that remove the incident laser reflection sufficiently. A piezoelectric stage was introduced to shift the position of the grating for changing the illumination phase.

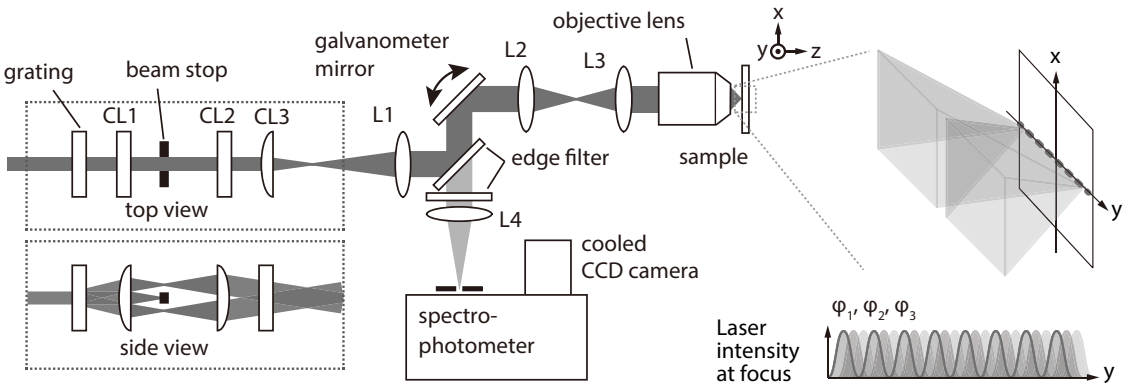

Fig. 3-4 Constructed optical setup of SLI Raman microscope.

Image processing for SLI Raman microscope

After data acquisition, the obtained data set is applied pre-processing: bias removal, cosmic ray removal, and pixel resampling. The pre-processing of the dataset is applied in the way, which is described in the literature [6]. A SIM image reconstruction, which is described in Chapter 1.3, is then performed to extract the high spatial frequency information from the pre-processed data set [7]. For the extraction of the high-spatial frequency information, the illumination phase have to be determined, however, the precise knowledge of the phase information is difficult for the actual experimental situation. Therefore, I estimated the initial phase by applying the different initial phase information and determine the value by comparing the resulting images, so that the image doesn't show image artifact. Also, the OTF compensation, which is described in chapter 2, is applied using Wiener filter. The value of the Wiener parameter is generally determined empirically. Therefore, I determined Wiener parameter by checking the resultant images, applying the different OTF compensation filter with different Wiener parameter. Finally, noise reduction utilizing SVD and baseline correction by polynomial curve fitting are applied in the spectral dimension in order to improve the signal-to-noise ratio (SNR) and to remove the broad-band background mainly by fluorescence, respectively.

Unlike the image processing for conventional SIM and Raman microscopy, the data set is treated with pixel resampling. Resampling in the spectral axis is required to compensate image distortion induced in the imaging spectrophotometer. Fig. 3-5a shows the spatial frequency spectra of the thin fluorescent film before the pixel resampling. The fluorescence film is illuminated by the structured line illumination, and fluorescence from the sample is imaged by the 0th order diffraction in the spectrophotometer. Then one-dimensional image along y axis is divided into 8 sections. Fourier transform of each section clearly shows the variation of spatial frequencies at the different detector positions as shown in fig. 3-5b. The solid line in fig. 3-5b shows the result of polynomial fitting of the detected spatial frequency. Based on the fitting result, the pixel sizes of the each position are compensated using a resampling algrithm. After the pixel resampling, the peak shift of the spatial frequency at different position is compensated as shown in fig. 3-5c.

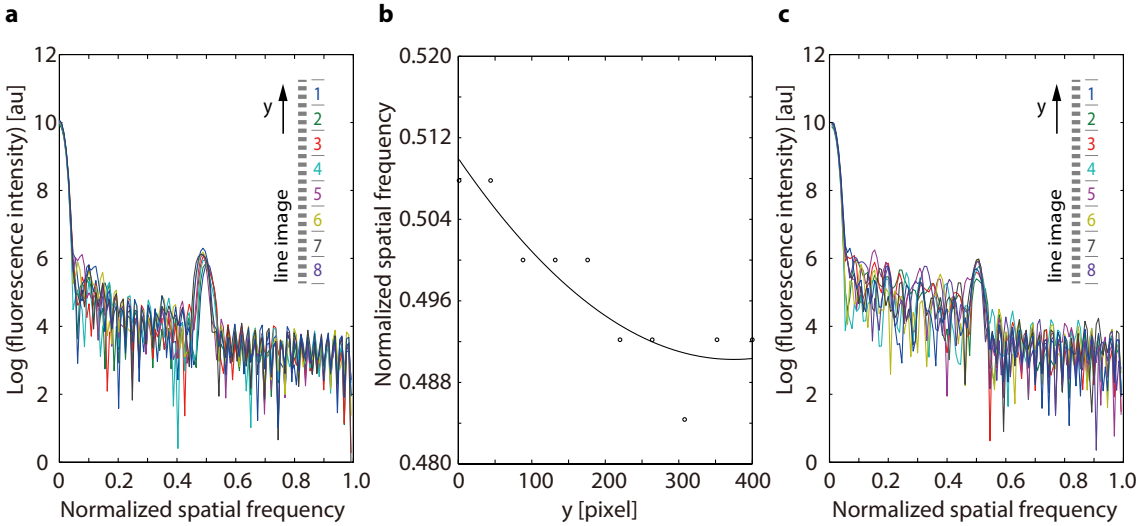

Fig. 3-5 Compensation of the image distortion is needed for SIM imaging with spectrometer in order to eliminate the image distortion induced by spectrometer.

Evaluation of the spatial resolution in LI and SLI Raman microscopy

The spatial resolution obtained in the SLI Raman microscope was evaluated by fluorescence imaging of fluorescence particles with a diameter of 40 nm. Fig. 3-6 shows x and y profile of the particle obtained in LI and SLI modes. The profiles of 10 isolated fluorescence particles were averaged for the comparison.

The FWHM of the profiles are following:

LI: x) 281 nm, y) 366 nm / SLI: x) 288 nm, y) 199 nm

FWHM of y-axis shows 1.8 times resolution improvement in SLI microscope, while x-axis doesn't show significant difference.

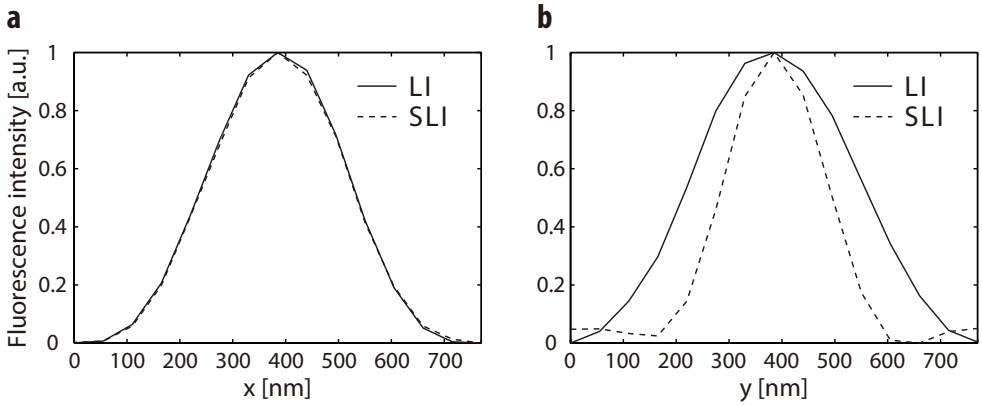

Fig. 3-6 The x and y profiles of the images of fluorescence beads with a diameter of 40 nm obtained by the LI and SLI Raman microscopes. 10 images of isolated fluorescence beads are averaged for the comparisons.

The improvement of the spatial resolution was confirmed at wide range of the wavenumbers measured in the experiment. Fig. 3-7 shows three-dimensional spatial frequencies of the Raman scattering data stack of polystyrene particles with a diameter ϕ of 330 nm. The comparison between the spatial frequencies obtained in the LI and SLI microscopes clearly shows the expansion of detectable spatial frequency limit at different wavenumbers using the SLI Raman microscope.

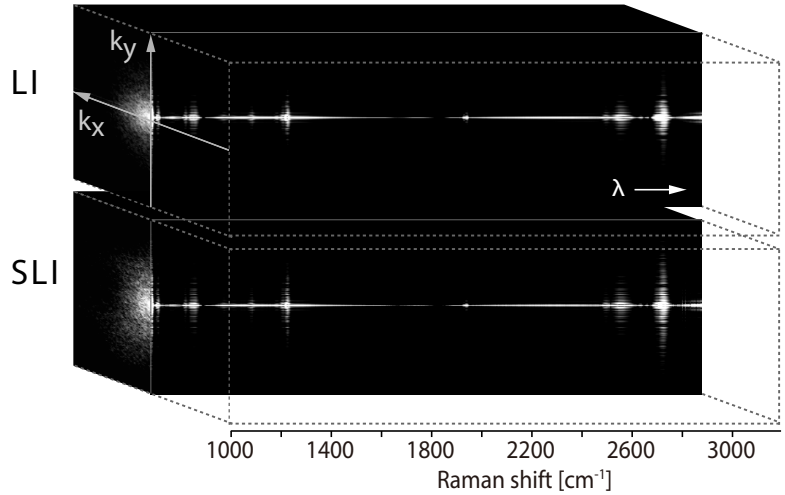

Fig. 3-7 Spatial frequencies of the hyperspectral Raman images of polystyrene particles with a diameter of 330 nm obtained by the LI and SLI Raman microscopes, showing the improvement of the spatial resolution in wide range of the wavenumber region.

Although Fig. 3-6 doesn't show a resolution improvement in x-axis, resultant SLI

Raman image seem to have higher spatial resolution comparing with LI Raman image (Fig. 3-8). In order to check the effect of Wiener filter used for the OTF compensation in the SIM image reconstruction, which is described above, I compared the profiles of Raman images of polymer nanoparticles. Fig. 3-8a, c shows the Raman images of ϕ500 nm polystyrene (PS) particles and ϕ800 nm poly(methyl methacrylate) (PMMA) particles imaged with the LI and SLI Raman microscope. The LI image is reconstructed by averaging the three images taken with different illumination phase. Fig. 3-8b shows the Raman image of LI after applying the same Wiener filtering to y-axis used in the SIM reconstruction process. Checking the x-profile of PS particles, the image size of an isolated PS particle is identical (Fig. 3-8e). However, the profile of a PS particle having adjacent particles (Fig. 3-8f) shows the improved suppression capability of the contribution of adjacent particle, which may result in the effect of Wiener filtering in y-axis. Although the Wiener filtering does not improve the two-points resolution, the effect of the sharpened outer edge of the particle is also shows in fig. 3-8d.

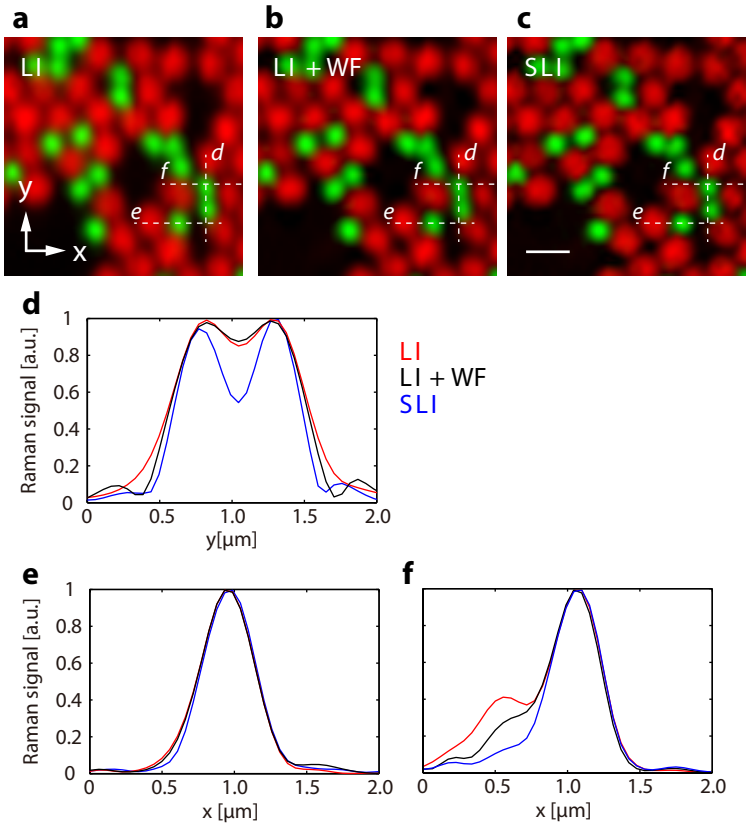

Fig. 3-8 a-c Raman images of PS and PMMA particles with different imaging modes (LI, LI+Wiener filter (WF), and SLI). d-f Comparison of the images of PS particles in **a-c**.

3.3 Experimental results of SLI Raman microscopy

Using the developed SLI Raman microscope, I observed various kinds of samples: polymer nanoparticles, few layer graphene, graphite, mouse brain tissue, and fixed HeLa cell. In this chapter, the practical application of SLI Raman microscopy is shown.

Polymer nanoparticles

Molecular structures of polymer show the strong Raman scattering, and Raman microscopy can be used to examine the defect of the polymer sample. Fig. 3-9 shows Raman spectra obtained from pure PS and PMMA particle. The assignments of each Raman band is cited from the reference [8]. Fig. 3-10 shows the Raman images of PS and PMMA particles. The images are constructed by the Raman shift indicated in Fig. 3-9, which can show the distribution of pure PS and PMMA. Bottom images in Fig. 3-10 shows magnified images in dotted region of upper images, and the plot shows the profiles of the PS particles between indicated arrows in the figure. As seen from the comparison between the LI and SLI image, I obtained enhanced spatial resolution for the all field of view.

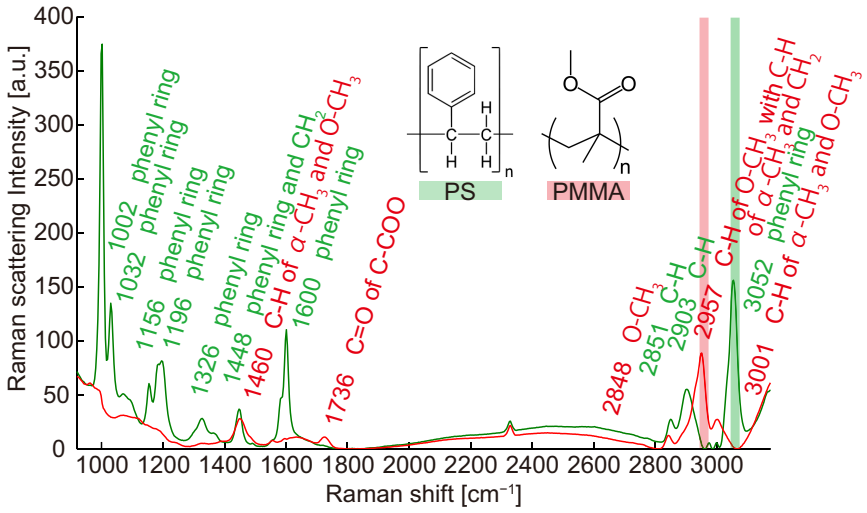

Fig. 3-9 Raman spectra obtained from PS and PMMA [8].

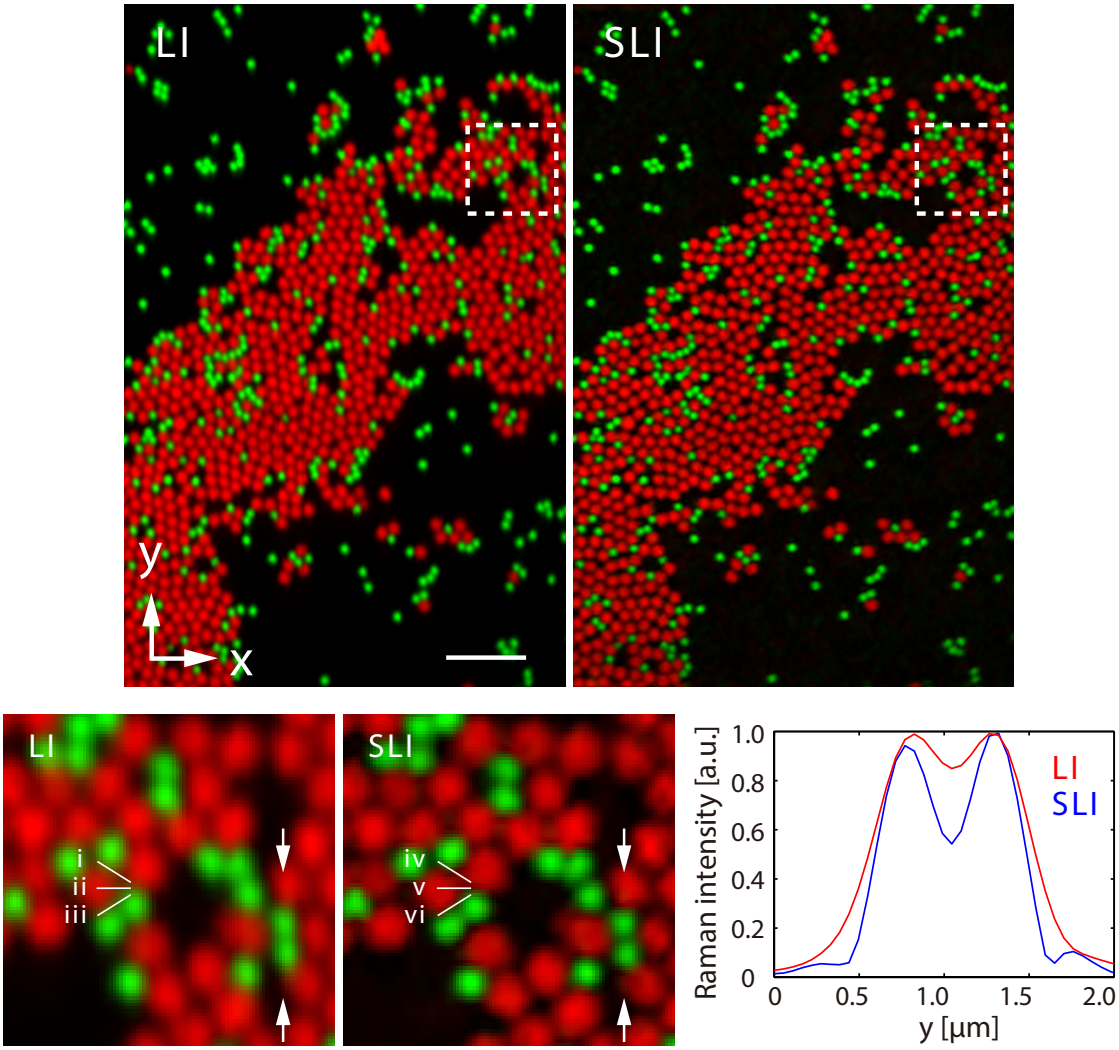

Fig. 3-10 LI and SLI Raman images of ϕ 500 nm PS (3055 cm-1, green) and ϕ 800 nm PMMA (2957 cm-1, red) nanoparticles.

In addition to the resolution improvement, SLI Raman microscope shows higher capability to separate Raman spectra from different species. Fig. 3-11 shows Raman spectra from adjacent data points indicated in fig. 3-10. In the LI Raman image, Raman spectrum from i shows strong Raman peak at around 1000 cm^{-1} and 2900 cm^{-1}, which is typical Raman peak from PS and PMMA, respectively. Therefore, the Raman spectrum indicates the existence of both PS and PMMA molecules. Also ii, iii, are the mixture of the spectra of PS and PMMA. In contrast, in the SLI Raman image, spectra obtained from iv and vi, which is the same points of i, ii, iii, shows mostly identical Raman spectra of pure PS and PMMA spectra.

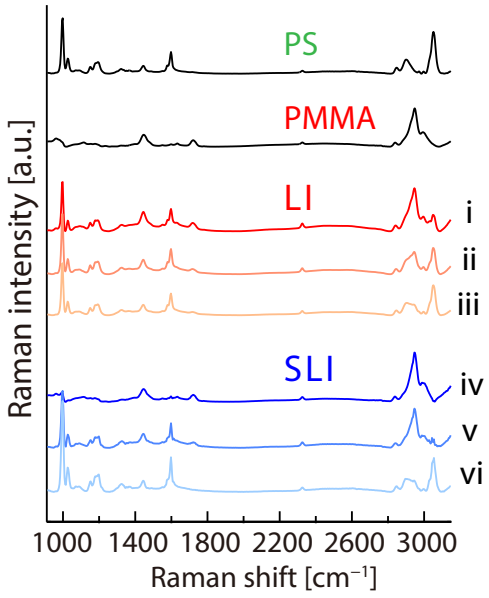

Fig. 3-11 Raman spectra obtained from different points in Fig. 3-10

Carbon materials: graphene and graphite

Graphene is expected as the next generation electronic material. Recently, the electrical circuit made of graphene is successfully fabricated [9]. For the analysis of the layer number or the distribution of the defect, Raman microscopy is widely used [10]. However, the conventional commercial Raman microscopy has a limited spatial resolution, which is far beyond the structure of carbon nano-materials. Thus, improvement of the spatial resolution in Raman imaging is desired for analysis of various carbon materials.

I observed a few-layer graphene by using developed SLI Raman microscope as shown in Fig. 3-12. We used a graphene sample fabricated by CVD [11]. The SLI Raman image clearly shows the reticulate distribution of D band with the improved spatial resolution. Fig. 3-13 shows the characteristic Raman spectra of graphene, which is obtained from SLI Raman image in Fig. 3-12. The enhanced spatial resolution can be seen from the profiles of D band in the line between the indicated arrows in Fig. 3-12 (Fig. 3-14).

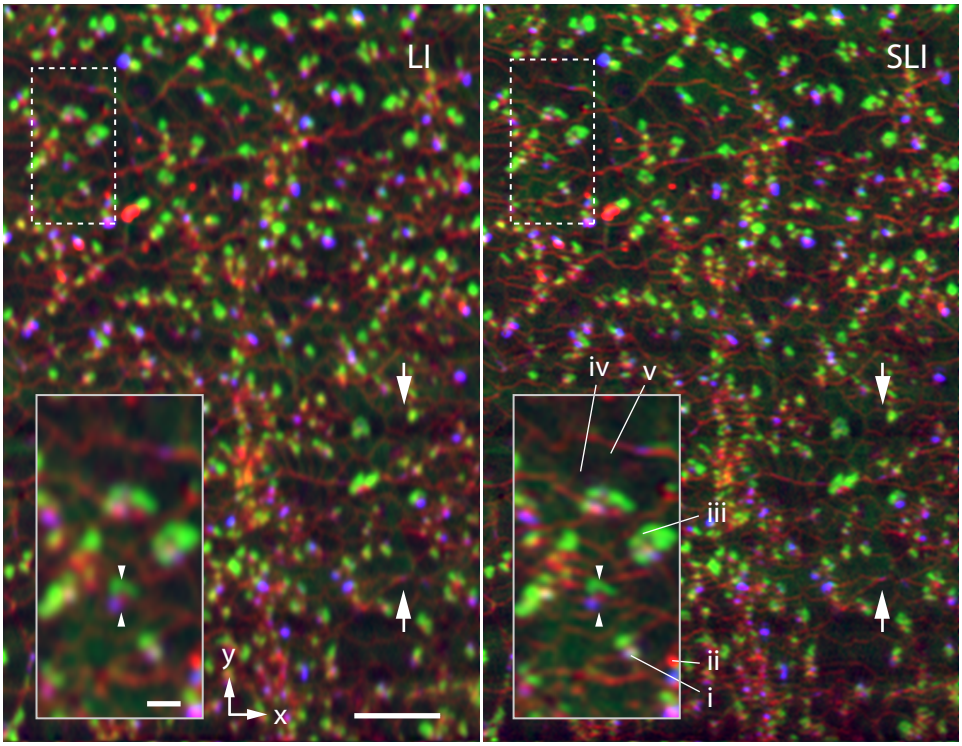

Fig. 3-12 SLI Raman image shows clearly higher spatial resolution image of reticular structured graphene. The image is constructed with D (1307-1387 cm^{-1} averaged, red), G (peak intensity seen at 1589-1598 cm^{-1}, blue) and 2D (peak intensity seen at 2682-2694 cm^{-1}, green) bands.

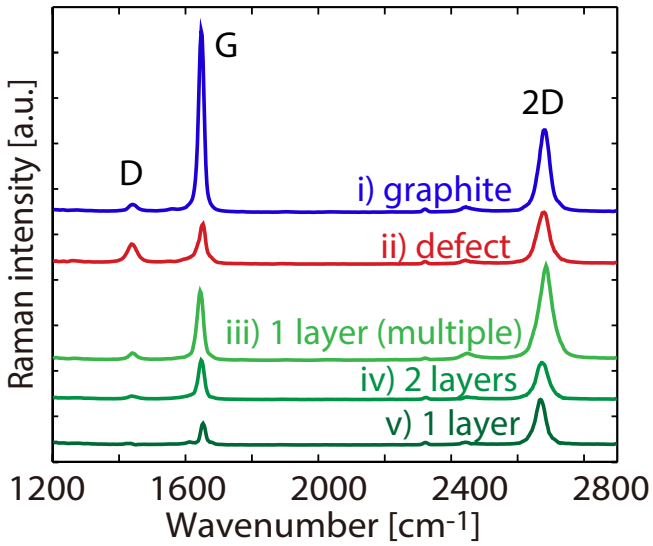

Fig. 3-13 Characteristic Raman spectra of graphene from the points indicated in Fig. 3-12.

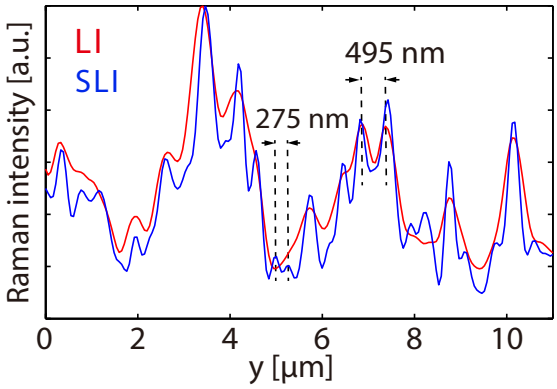

Fig. 3-14 Profile of D band intensity between indicated arrows in Fig. 3-12 shows obvious improvement of spatial resolution.

SLI Raman microscope shows the improved capability of Raman spectrum analysis as shown in the Raman imaging of PS and PMMA particle mixtures. Fig. 3-15 shows the variation of Raman spectra between the arrows indicated in the inset of fig. 3-12. In the SLI Raman spectra, the correlation between the distribution of D band and G band is clearly confirmed while no correlation with 2D band distribution, which was not observed in LI Raman microscopy.

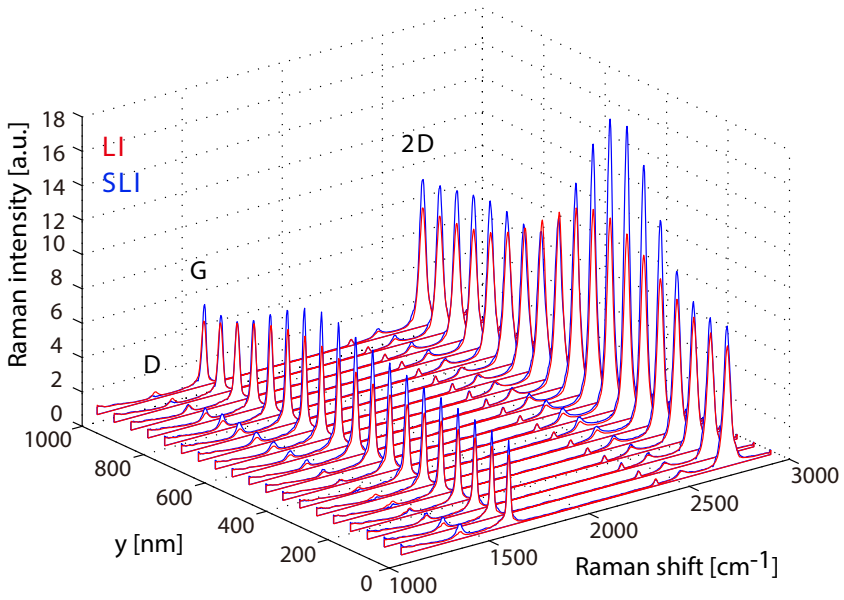

Fig. 3-15 The spatial variation of Raman spectra between the arrows indicated in the inset of Fig. 3-12

The graphite sample was also observed by the SLI Raman microscope. The sample

was prepared by mechanical exfoliation of graphite using the scotch-tape method [12], The detailed structure of the graphite surface can be clearly seen in SLI Raman image.

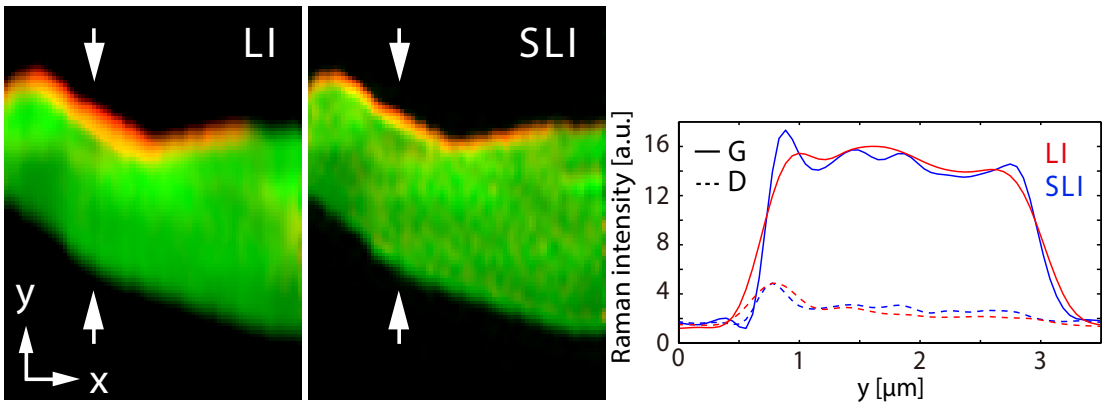

Fig. 3-16 LI and SLI Raman image of D (1340-1370 cm^{-1} averaged, red) and G (1543-1611 cm^{-1} averaged, green) band distribution in graphite.

Mouse brain tissue and HeLa cells

Raman analysis of biological samples also attains much interest for its capability of the label-free imaging and the capability to distinguish the complex biological strucutres using rich molecular information in the Raman spectrum.

I observed a mouse brain tissue by the SLI Raman microscope. For the sample preparation, an adult male C57BL/6 mice were anesthetized with sodium pentobarbital (50 mg kg-1, intraperitoneally), and perfused through the left ventricle with 4% paraformaldehyde in phosphate-buffered saline (4% PFA). Brains were removed, fixed overnight at 4°C in 4% PFA, and sliced at a thickness of 20 μm in phosphate-buffered saline on a Leica vibratome (VT 1000S). Animal experiments were performed in accordance with the guidelines of the Japanese Pharmacological Society, and were approved by the Animal Care and Use Committee of the Graduate School of Pharmaceutical Sciences, Osaka University.

Fig. 3-17 shows the images constructed by using the vibrational mode of amide-I, which can be assigned to the vibration of protein beta sheets, and CH_2 stretching mode, which is mainly distributed in lipids, Bundles of neural fibers with lipid-rich myelin sheaths connecting the two cerebral hemispheres in the corpus callosum are clearly resolved only in the SLI image constructed with the CH_2 stretching mode (Fig. 3-17).

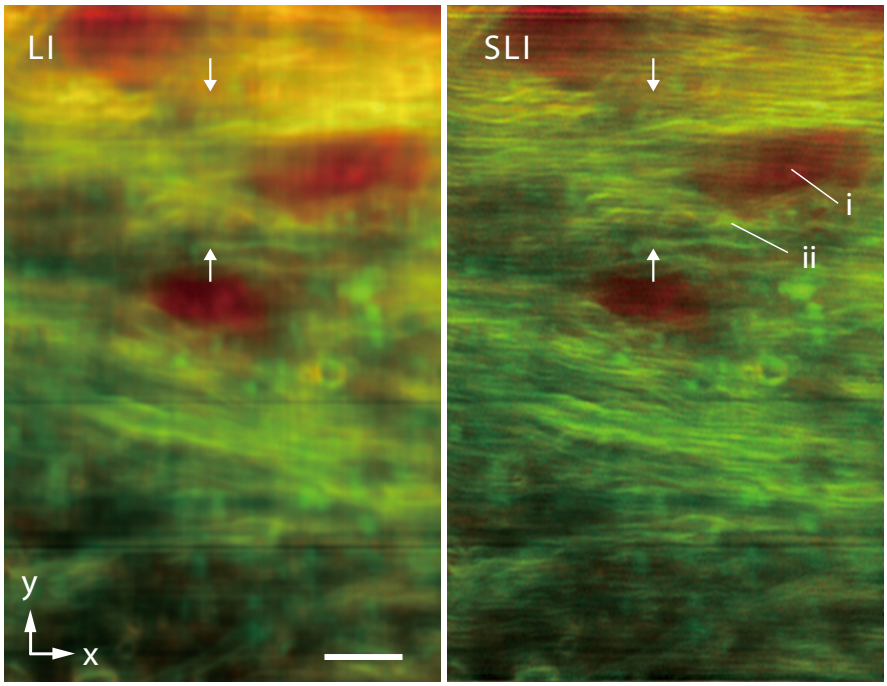

Fig. 3-17 Raman image of coronal section of sliced mouse brain tissue in LI and SLI Raman microscope in show in in amide-I (1682 cm-1, red) and CH2 stretching (2848 cm-1, green).

Characteristic spectral differences between different data points are shown in the Fig.3-18. The Raman scattering intensity profiles at the wavenumber at 2848, 2884, 2930 cm^{-1}, whose intensity distribution can be used for characterizing different protein distribution (Fig. 3-2), clearly indicate higher spatial resolution in SLI Raman microscope (Fig. 3-19). For example, Raman scattering intensity ratio of 2845 cm^{-1} and 2930 cm^{-1} is used to visualize the tumor cell distribution in the mouse brain sample, since the intensity ratio difference reflects the difference of the protein and lipid concentration at the detection point [13]. Also, Raman scattering intensity ratio of 2849 cm^{-1} and 2884 cm^{-1} is used for characterizing the specific phospholipids folding in multilamellar dispersions [4]. These observed results show the enhanced potential of the Raman microscopy for the detailed diagnosis of biological specimens.

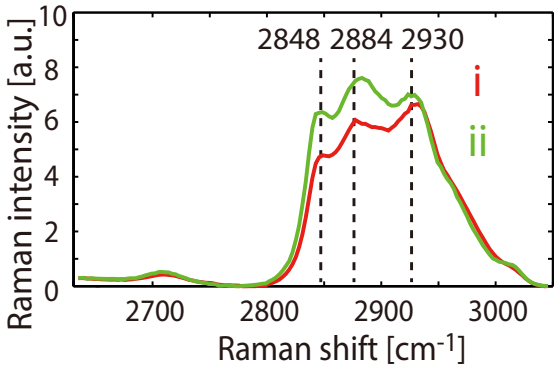

Fig. 3-18 Raman spectra from the points indicated in SLI Raman image (Fig. 3-17)

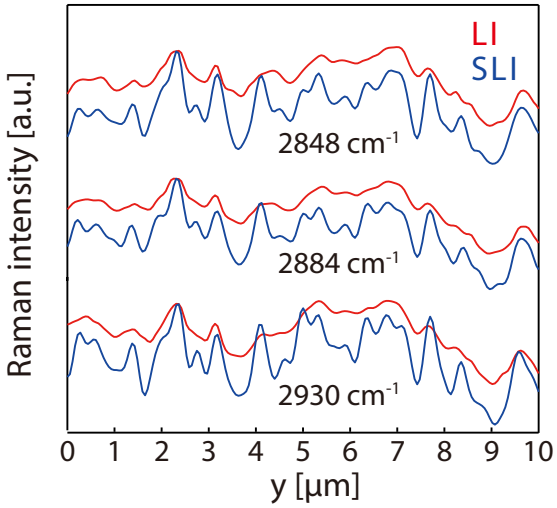

Fig. 3-19 The Raman scattering intensity profile between indicated arrows in fig.3-16 shows clear spatial resolution improvement in SLI Raman microscope to LI Raman microscope

I observed fixed HeLa cell using LI and SLI Raman microscope. HeLa cell sample were fixed using PFA, and illumination intensity of 2 mW/μm^2 and exposure time of 5 sec/line was used for the observation. Fig 3-20 shows the Raman image of the HeLa cell with 2848 cm^{-1}, which shows the distribution of the lipid. The adjacent lipid droplet inside the HeLa cell is more clearly separated in SLI Raman microscope.

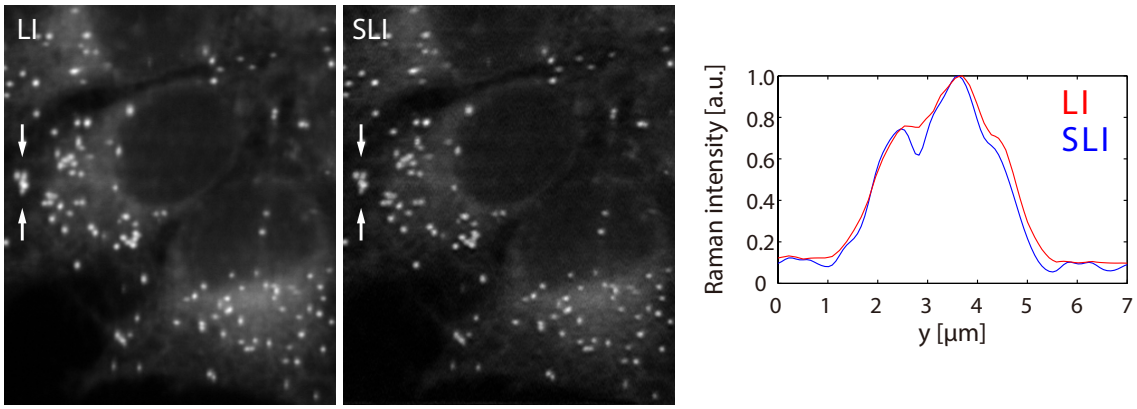

Fig. 3-20 Comparison of the LI image and SLI Raman image. Images were constructed using Raman intensity at 2848 cm^{-1} to show the distribution of the lipid.

Discussion

In these experiments, the use of SLI in Raman microscopy shows not only the improvement of spatial resolution but also the enhanced capability of discriminating spectrum components, which is advantageous for analysis of multi-component samples of which Raman spectra are typically complicated. For these types of samples, it is common to apply multivariate analysis to extract valuable information from the mixture of Raman scattering. The high spectral discrimination capability of SLI Raman microscopy will help uncover original spectral features more efficiently and reliably from the mixed Raman spectra.

The improvement of spatial resolution is only valid in the direction parallel to the illumination line in SLI Raman microscopy. On the other hand, the spatial resolution in the perpendicular direction is limited by the slit width of the spectrophotometer. As discussed in Chapter 2.2, SLI microscopy has a trade-off in x and y spatial resolution because as the structured illumination becomes more closely spaced, the line focusing itself becomes less tightly focused. In our experimental conditions, the normalized offset distance, which is given as the ratio of the spatial frequency of the illumination fringe to the cut-off frequency in the illumination optics, is 0.56 (for the dry objective lens) and 0.48 (for the water immersion objective lens). These illumination conditions offer nearly isotropic spatial resolution in the lateral directions and 1.4-fold improvement of the spatial resolution along the slit direction compared to the theoretical cut-off in wide-field microscopy.

From the view pint of the comparison between SLI Raman microscopy with point

scanning confocal Raman microscopy, it is known that the infinitely small detection pinhole in confocal microscopy can provide 1.4 times resolution improvement. However, in the actual experimental condition, the detection pinhole size of around 0.5 Airy disc units in fluorescence microscopy, and around 1 Airy disc unit for Raman microscopy are generally used. The large detection pinhole size is used for the Raman imaging, since the Raman scattering is very weak and it is not practical to use infinitely small detection pinhole. In the SLI Raman microscopy, I used the detection slit width of 1 Airy unit, therefore it ensures high-resolution Raman image with relatively high SNR.

According to the discussion in chapter 2 and reference [14], the Ar of ~0.8 will provide high resolution in x- and y-axis without the degradation of z-resolution. The use of high Ar will be advantageous for the samples, which require higher resolution and can accept long image integration time. There are two reasons for this: First, the Ar of 0.8 requires the rotation of the illumination pattern, thus the image integration time is three times longer. Second, the separation of high spatial frequency information requires high SNR in raw images; therefore, the image integration time for one raw image may be longer. In this study, I designed the optics so that the image integration time is practically acceptable time scale. It is desirable to design the optics for the specific applications.

The design of SLI Raman microscopy for the practical application, the image integration time and the possible techniques to overcome the long integration time should be discussed. One solution for that is the use of wide-field Raman microscopy. It is also possible to implement the structured pattern in wide-field illumination instead of line illumination, and wide-field illumination can provide faster image acquisition compared to SLI. In this study, the spectrophotometer is used for the hyperspectral Raman imaging. It can be possible to eliminate the scanning of the illumination pattern, and illuminate the sample with two-dimensional structured illumination pattern. The use of the line illumination and the spectrophotometer allows us to obtain the rich information of the Raman bands; therefore, it has advantages for the analytical imaging. The other possibility to shorten the image integration time is by the acquisition of the different illumination phase data at the same time. There are two possibilities for that, which utilize the polarization or the color of the light. Until now, it is reported that utilizing the polarization of the illumination light, it is possible to obtain the three different illumination phase images at the same time [15]. Also it is reported that the multi-color excitation can be used for the simultaneous detection [16]. However, the applications of these

methods are limited to the specific samples, which don't have polarization of wavelength dependent Raman scattering characteristics. Also, the experimental parameters should be carefully chosen for the experiment.

It is also important for the current development of the Raman microscopy techniques to infer the coherent Raman imaging, such as coherent anti-Stokes Raman scattering (CARS) or stimulated Raman scattering (SRS). The coherent Raman imaging is considered as the emerging powerful analytical imaging tool, because of the capability of the high-speed Raman imaging utilizing the enhanced Raman effect. Generally, CARS microscopy setup utilizes confocal microscopy system. Because of its third-order nonlinearity Raman effect, it is expected to provide high-resolution imaging. In contrast, practical CARS microscopy uses NIR light source, therefore, practical spatial resolution in CARS microscopy is not high compared to the spontaneous Raman microscopy. Our SLI Raman microscopy enables quantitative and high-resolution spectral imaging.

It is also important to refer the application of the SLI Raman microscopy. As it is discussed, Raman microscopy is a powerful tool for the observation in the various scientific fields, such as polymer composites, carbon materials, biological tissues, and pharmaceutical tablets. SLI Raman microscopy can be the powerful analytical imaging tool for observing such samples with smaller spatial resolution than 200 nm. For example, the device improvement utilizing carbon nanostructures, such as graphene or carbon nanotube, are emerging techniques. The graphene devices are recently came to be realized [9][17]. Such kind of graphene devices, with hundred nanometer order structures may require high-resolution and large area analytical observation for the characterization and the inspection of the fabricated structure. In addition, although the carbon materials are expected to be the next-generation device materials, the mechanism of the graphene sheet growth has been under the discussion [18]. SLI Raman microscopy can be contribute to such a fundamental questions for the material sciences. In the biological sample, SLI Raman microscopy can be used for the alternative imaging methods with fluorescence microscopy of electron microscopy. Fluorescence microscopy can obtain the distribution of the specific molecule using the fluorescence tag, which is attached to the specific molecules, with high resolution and high temporal resolution. In contrast, although the resolution and the image acquisition speed of Raman microscopy are not very high, Raman microscopy can visualize the characteristics of the molecular structure itself. Recently, it is

reported that the different protein can be distinguished by the Raman spectrum without dying the sample [19]. It had been also reported to distinguish the stacking order of the lipid bilayer [4], which is quite difficult to distinguish by fluorescence imaging. In combination of the information that can be obtained with different imaging modality, such as fluorescence microscopy or scanning electron microscopy, it is possible to access to the information that cannot be realized before. Finally, in the pharmaceutical material, it has been difficult to know the distribution of the specific components. Raman microscopy can spectrally distinguish the difference of the pharmaceutical components, thus, it will open up the future development of drug.

References

[1] R. C. V. and K. K. S., "A New Type Of Secondary Radiation," *Nature*, vol. 121, no. 3028, p. 501, 1928.

[2] 濱口宏夫・平川暁子、『ラマン分光法』、学会出版センター、1988.

[3] A. F. Palonpon, M. Sodeoka, and K. Fujita, "Molecular imaging of live cells by Raman microscopy.," *Curr. Opin. Chem. Biol.*, pp. 1–8, Jun. 2013.

[4] C. Huang, J. T. Mason, and I. W. Levin, "Raman spectroscopic study of saturated mixed-chain phosphatidylcholine multilamellar dispersions.," *Biochemistry*, vol. 22, no. 11, pp. 2775–2780, 1983.

[5] K. Watanabe, A. F. Palonpon, N. I. Smith, L. Chiu, A. Kasai, H. Hashimoto, S. Kawata, and K. Fujita, "Structured line illumination Raman microscopy," *Nat. Commun.*, vol. 6, no. May, p. 10095, 2015.

[6] A. F. Palonpon, J. Ando, H. Yamakoshi, K. Dodo, M. Sodeoka, S. Kawata, and K. Fujita, "Raman and SERS microscopy for molecular imaging of live cells," *Nat. Protoc.*, vol. 8, no. 4, pp. 677–692, Mar. 2013.

[7] M. G. L. Gustafsson, L. Shao, P. M. Carlton, C. J. R. Wang, I. N. Golubovskaya, W. Z. Cande, D. a Agard, and J. W. Sedat, "Three-dimensional resolution doubling in wide-field fluorescence microscopy by structured illumination.," *Biophys. J.*, vol. 94, no. 12, pp. 4957–70, Jun. 2008.

[8] K. J. Thomas, M. Sheeba, V. P. N. Nampoori, C. P. G. Vallabhan, and P. Radhakrishnan, "Raman spectra of polymethyl methacrylate optical fibres excited by a 532 nm diode pumped solid state laser," *J. Opt. A Pure Appl. Opt.*, vol. 10, no. 5, p. 055303, May 2008.

[9] S. Han, A. V. Garcia, S. Oida, K. A. Jenkins, and W. Haensch, "Graphene radio frequency receiver integrated circuit," *Nat. Commun.*, vol. 5, pp. 1–6, 2014.

[10] J. Tsurumi, Y. Saito, and P. Verma, "Evaluation of the interlayer interactions of few layers of graphene," *Chem. Phys. Lett.*, vol. 557, pp. 114–117, Feb. 2013.

[11] Z. Sun, Z. Yan, J. Yao, E. Beitler, Y. Zhu, and J. M. Tour, "Growth of graphene from solid carbon sources.," *Nature*, vol. 468, no. 7323, pp. 549–52, Nov. 2010.

[12] K. S. Novoselov, A. K. Geim, S. V. Morozov, D. Jiang, Y. Zhang, S. V. Dubonos, I. V. Grigorieva, and A. A. Firsov, "Electric Field Effect in Atomically Thin Carbon Films," *Science (80-.).*, vol. 306, pp. 666–669, 2004.

[13] M. Ji, D. a Orringer, C. W. Freudiger, S. Ramkissoon, X. Liu, D. Lau, A. J. Golby, I.

Norton, M. Hayashi, N. Y. R. Agar, G. S. Young, C. Spino, S. Santagata, S. Camelo-Piragua, K. L. Ligon, O. Sagher, and X. S. Xie, "Rapid, label-free detection of brain tumors with stimulated Raman scattering microscopy.," *Sci. Transl. Med.*, vol. 5, no. 201, p. 201ra119, Sep. 2013.

[14] T. Kim, D. Gweon, and J.-H. Lee, "Enhancement of fluorescence confocal scanning microscopy lateral resolution by use of structured illumination," *Meas. Sci. Technol.*, vol. 20, no. 5, p. 055501, May 2009.

[15] K. Wicker and R. Heintzmann, "Single-shot optical sectioning using polarization-coded structured illumination," *J. Opt.*, vol. 12, no. 8, p. 084010, Aug. 2010.

[16] L. G. Krzewina and M. K. Kim, "Single-exposure optical sectioning by color structured illumination microscopy.," *Opt. Lett.*, vol. 31, no. 4, pp. 477–479, 2006.

[17] S. Han, A. Valdes-garcia, A. A. Bol, A. D. Franklin, D. Farmer, E. Kratschmer, K. A. Jenkins, and W. Haensch, "Graphene Technology with Inverted-T Gate and RF Passives on 200 mm Platform," *Electron Devices Meet.*, pp. 19–22, 2011.

[18] Q. Yu, L. a Jauregui, W. Wu, R. Colby, J. Tian, Z. Su, H. Cao, Z. Liu, D. Pandey, D. Wei, T. F. Chung, P. Peng, N. P. Guisinger, E. a Stach, J. Bao, S.-S. Pei, and Y. P. Chen, "Control and characterization of individual grains and grain boundaries in graphene grown by chemical vapour deposition.," *Nat. Mater.*, vol. 10, no. 6, pp. 443–9, Jun. 2011.

[19] a. Rygula, K. Majzner, K. M. Marzec, a. Kaczor, M. Pilarczyk, and M. Baranska, "Raman spectroscopy of proteins: a review," *J. Raman Spectrosc.*, vol. 44, no. 8, pp. 1061–1076, 2013.

Chapter 4
Spot illumination for structured illumination microscopy

In this chapter, the application of SIM to spot illumination is discussed. The enhanced capability to suppress the out-of-focus signal by spot-illumination expands the potential of super-resolution microscopy to observe thick fluorescent samples. The two-photon excitation fluorescence imaging, as well as the one-photon excitation, further expands the possibility to image deep tissue with high spatial resolution. The theoretical imaging characteristics of the non-linear structured illumination microscopy and the improvement of the spatial resolution are discussed.

4.1 Thick fluorescent sample imaging by structured spot illumination

The optical sectioning capability of optical microscopy is quite important for imaging the biological specimen. The emergence of confocal microscopy as a novel method to image inside the cell had expanded the capability of biologists to study the morphology and the dynamics of each biological function. The multi-focus imaging with multiple number of focus spots, further expands the optical sectioning imaging with high-acquisition speed. The use of multi-focus microscopy is a convenient choice to image fast biological dynamics with a few hundred of nanometer resolution in all directions, with a relatively simple setup. In 1990, two-photon microscopy emerged as a tool to realize deep-tissue imaging.

In 1996, a method to enhance the axial resolution with structured illumination also emerged as a high-speed microscopy with optical sectioning capability [1] Efforts have been also made to enhance the axial resolution in optical microscopy, such as 4Pi microscopy and I^5M microscopy [2][3]. It enabled imaging the sample even with the axial resolution of sub-hundred nanometers. In addition, super-resolution has expanded its applications to three-dimensional microscopy, such as 3D-STED, and it became possible to image the sample with high lateral spatial resolution and axial resolution. However, the practical application of such method to thick fluorescent samples is challenging, since it is difficult to control the illumination spot shape in such a small area. The efforts to image the sample with high three

dimensional resolution are still continuing until now.

The application of SIM to thick fluorescent samples has been essentially limited because wide-field system doesn't have optical sectioning capability. The practical application of the wide-field SIM to thick fluorescent sample has been limited to the thickness of ~20 μm [4]. However, the realization of SIM with optical sectioning enables high-speed imaging with relatively high lateral resolution. The different configurations to overcome the limitation of the thick sample imaging are discussed in the reference [5]. The first possibility is SLIM, which is studied in Chapter 2. This approach can increase the optical sectioning capability by the removal of out-of-focus by the image processing or physical slit; however, the achievable spatial resolution is limited in consideration of the balance between lateral resolution and axial resolution. In addition, the optical setup is complicated and it is not practically reasonable to equip SLIM for fluorescence imaging. The second possible configuration is light-sheet geometry [6]. Light-sheet microscopy typically uses two vertically positioned objective lenses: one for the illumination and another for the detection. Since thin light sheet illuminates only the detection area, the out-of-focus contribution can be suppressed. However, difficulty of the appropriate mounting for the light-sheet configuration may restrict the practical application for the observation of the specimen. The third possibility is the application of SIM to multi-focus system, which is commonly called instant-SIM technique [7]. This technique uses a simple observation system with spinning-disc setup to achieve the resolution, which is similar to SIM; however, the achievable resolution enhancement is degraded by the low modulation depth of the illumination pattern compared to the normal sinusoidal SI created by two or three beam interference. The fourth possibility is spot illumination combined with SIM, which is discussed in this chapter. Instead of wide-field illumination SIM, spot illumination uses loosely focused illumination at the sample (Fig. 4-1). Owing to the focusing of the illumination, the out-of-focus light can be largely reduced comparing with wide-field illumination. In addition, the interference of the incident beam with large angle assures strong modulation depth of SI pattern.

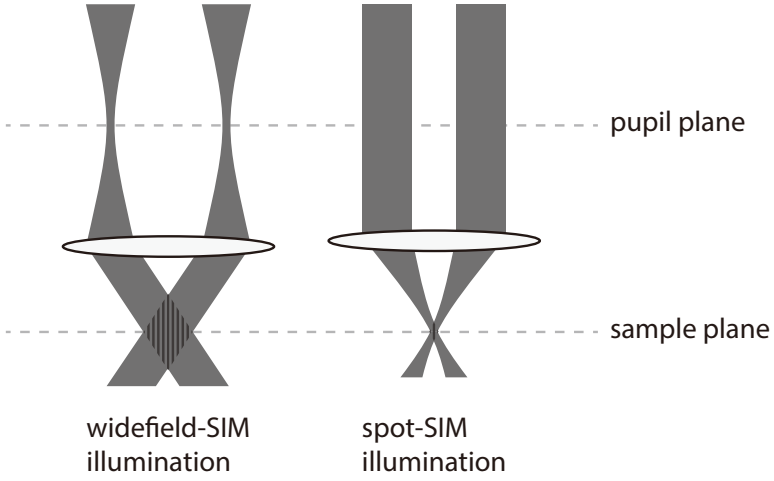

Fig. 4-1 The schematics of structured illumination with wide-field illumination and spot illumination system. Two loosely focused spots are superposed at the sample plane to form interference pattern.

Non-linear excitation of the fluorophore can also be enabled by the high-excitation intensity resulting from the use of focused illumination light. Two-photon microscopy using NIR laser for excitation is an important tool for the observation of deep tissue sample [8]. High-excitation intensity can be achieved by the focusing of the illumination beam. Since scattering of the light can be decreased by the use of longer wavelength, NIR excitation is advantageous to image the deep tissue because of the long penetration depth. The combination of two-photon microscopy with spot-SIM enables high-resolution deep-tissue imaging. Two-photon excitation Instant-SIM has been reported by M. Ingaramo in 2014 [9]. The study showed increased potential of imaging the sample with high lateral and axial resolution. Two-photon spot-SIM will further expand its potential to high SNR and higher spatial resolution imaging.

The image formation of the one-photon Spot-SIM is identical to wide-field SIM. However, the image formation in two-photon excitation fluorescence is different from that of one-photon case. In the next section, the image formation of two-photon SIM is discussed.

4.2 Two-photon structured spot illumination microscopy (Spot-SIM): Image formation

Fig. 4-2 shows the schematics of the spatial frequency information that can be obtained by two-photon SIM. The excitation OTF is illustrated in dotted lines, and the detection

OTF in the conventional microscopy is illustrated in solid lines. The detected signal contains higher order frequency peak as it is indicated in the dot, which will further expands the observable region. This schematics illustrates the second-order nonlinearity, however, higher order frequency peak can enhance the spatial resolution further [10].

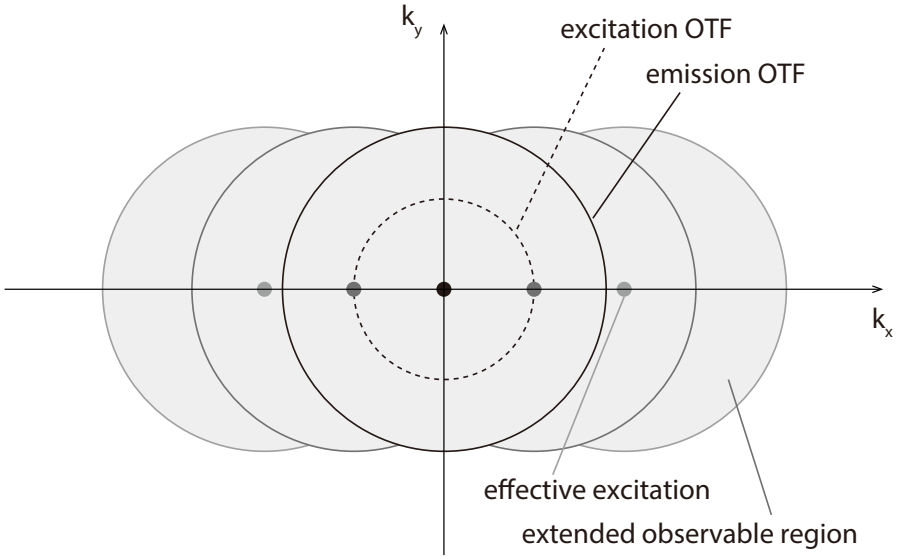

Fig. 4-2 The detectable spatial frequency information is enlarged by the effect of higher order SI frequency peak.

In the case of NIR excitation two-photon microscopy, we can take advantage of thick fluorescent samples. However, the resolution improvement in NIR two-photon microscopy is in the range of ~200 nm, because of the long excitation wavelength. It is also possible to use shorter excitation wavelength to increase the spatial resolution. It is reported that visible wavelength can be used for two-photon microscopy, since there is an absorbance band in the UV region [11]. Using the visible wavelength, multi-color imaging of the living cell sample can be enabled. Fig. 4-3 shows the energy diagram of fluorophores, which has absorption at UV region. As also shown in Fig. 4-3, many different kinds of fluorophores have absorption bands in the UV region. Therefore, it is also possible to excite different kinds of fluorophores by a single wavelength. Although UV wavelength one-photon excitation fluorescence microscopy is advantageous for high-resolution and multi-color imaging, it has been difficult to use UV light for the excitation, because of the large photo-damages caused by UV irradiation. Visible wavelength excitation can provide these advantages with low toxicity, because it can avoid unnecessary UV irradiation to the sample.

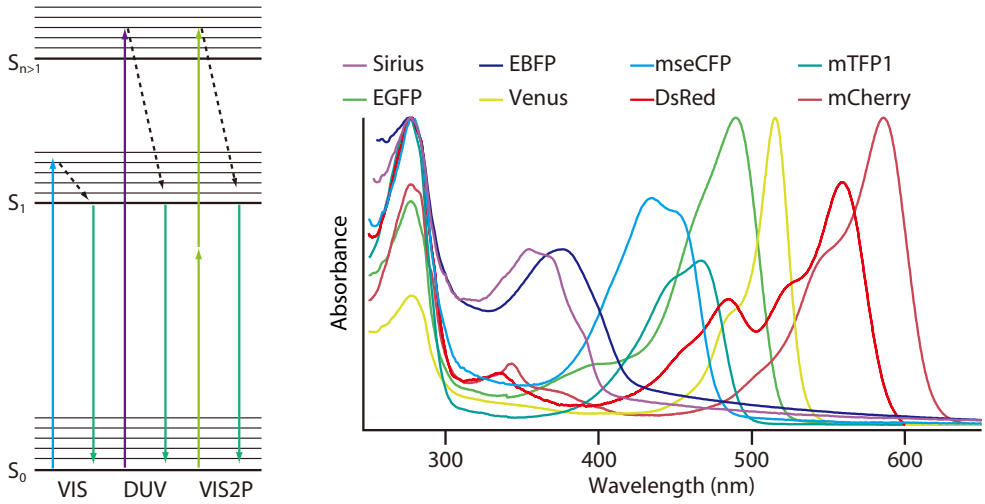

Fig. 4-3 Visible wavelength two-photon excitation can be used to excite many kinds of fluorescence proteins and fluorophores (Taken from [11]).

4.3 Optical sectioning property: theory and calculations

Depth resolution in one-photon excited spot-SIM

As described in the chapter 4-1, spot-SIM has advantages in depth-resolution. Here, the characteristic of the focus spot is discussed. In order to achieve the strong modulation depth of the illumination pattern, the polarization of the incident light should be maintained parallel to the grating. The schematic of the spot-SIM experimental setup is shown in Fig. 4-4. An incident laser beam is scanned in two-dimension using the galvanometer mirror to scan the spot illumination pattern at the sample plane. The linear polarizer is inserted in the first part of the setup to increase the polarization ratio, and then a quarter wave plate is put to make circular polarization. Both the linear polarizer and the following phase grating are mounted together on motors, and the motors change the angle and translational position to change the phase of the illumination pattern. These components keep the polarization parallel to the grating. The 0th order diffraction light is blocked by the following beam stop, and the +1st and -1st diffraction light form two-beam interference beam at the sample. The incident light is reflected by the dichroic filter and fluorescence from the sample is detected by CCD camera through the emission filter.

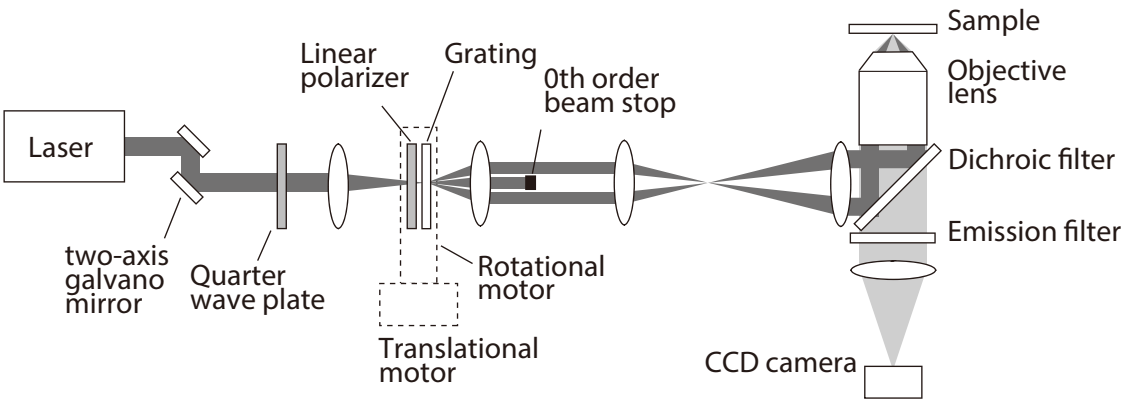

Fig. 4-4 An example of the optical setup of the spot-SIM

The depth resolution of the system is determined by the beam size of the +1st and -1st beam at the objective pupil. Since the relationship between the beam at the objective pupil and the sample plane is a Fourier transformation, therefore, smaller beam spots at the objective pupil make larger focus spots at the sample, and larger beam spots make smaller focus spots, thus higher depth focusing. Small beam spot at the objective pupil is used for the conventional large area illumination SIM.

Fig. 4-5 shows an example of the intensity distribution of the incident beam at the objective pupil. The dotted circle in the figure shows the edge of the excitation OTF. A FWHM of the beam width of 1 mm at the objective pupil is used for the calculation. The square root of the Fourier transformation of the amplitude distribution at the pupil plane derives the intensity distribution of the focus at the sample plane. As seen in fig. 4-5, the intensity distribution in spot-SIM forms a focused spot with grid pattern.

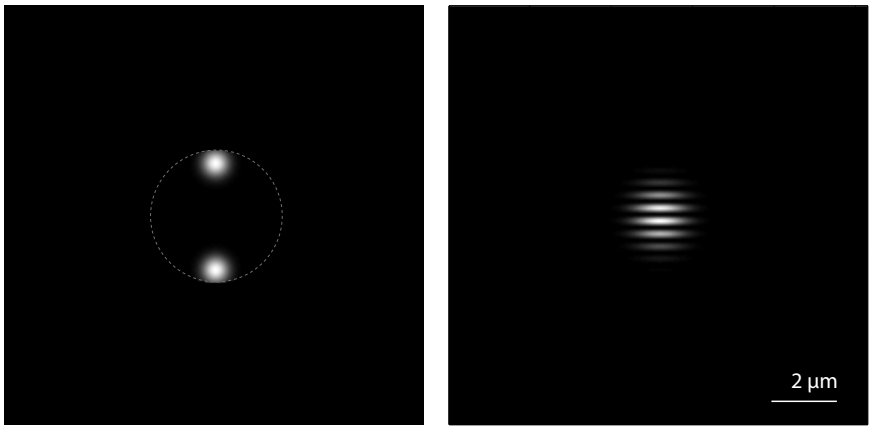

Fig. 4-5 The amplitude distribution of the incident beam at the objective pupil (left), and the intensity distribution at the sample plane (right).

The effective OTF is calculated the same way as shown in chapter 2-2, except the inclusion of the pinhole effect in the calculation. Also I considered the rotation to get the homogeneous resolution improvement in the lateral axis. Therefore, the PSF_{illu} is multiplied with PSF_{det} and then frequency information is shifted by k, and the process is repeated for the angle of 60 and 120 degrees. Fig.4-6 shows the intensity distribution of the focus light at the sample plane with different beam width at the objective pupil, whose diameter of 6.17 mm. It can be clearly seen that the larger beam width at the pupil effectively decreases the axial width of the focused pattern.

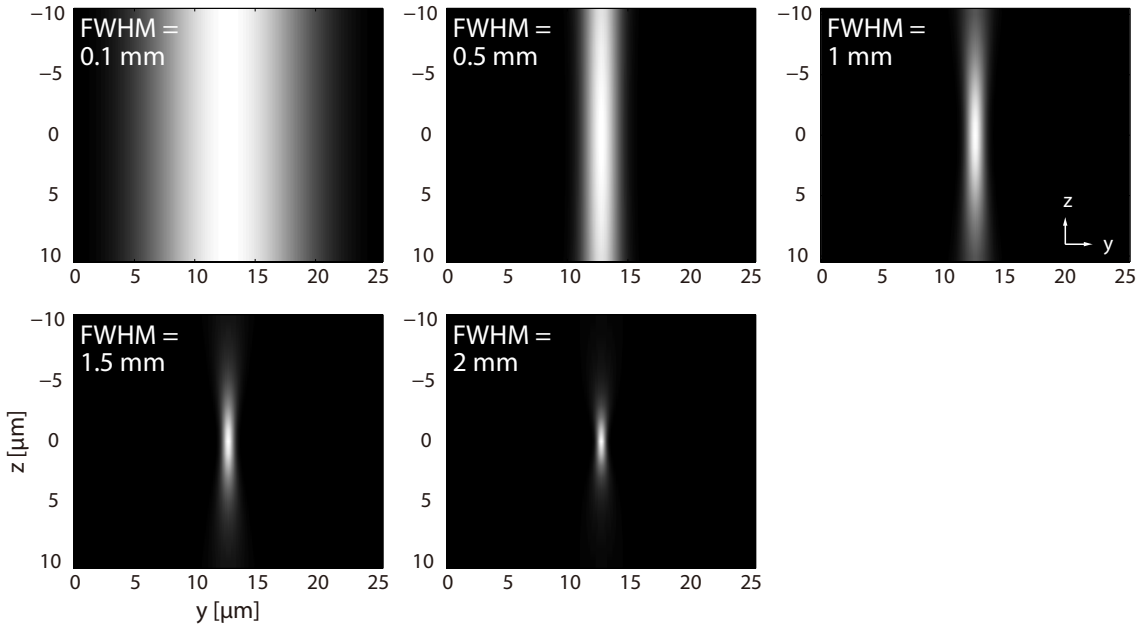

Fig. 4-6 The intensity distribution of the focus spot in yz plane with different beam width at the objective pupil.

I compared the y- and z-profile of the total OTF in spot-SIM with different beam width at the pupil (Fig. 4-7). The aperture ratio is kept constant Ar = 0.82 during the calculation. Comparison of the OTF profiles with different spot size shows the following tendency: as smaller the spot size at the objective focus, the axial spatial resolution, as well as the lateral resolution improved. This is because the tightly focused light suppresses the effect of the out-of-focus light contribution.

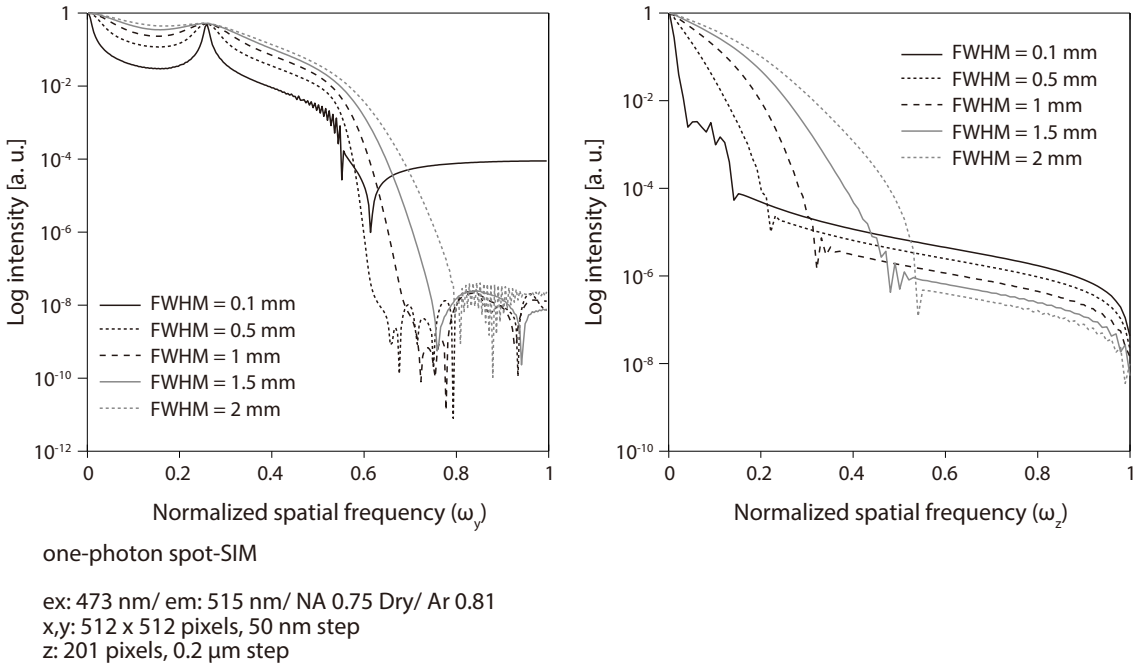

Fig. 4-7 The effective OTF in y- and z-axis with different beam width at the objective pupil.

Depth resolution in two-photon excited spot-SIM

The depth resolution in two-photon SIM with NIR and visible wavelength excitation can be calculated in the same way. In this case, PSF_{illu} is calculated by the square of one-photon PSF_{illu} to take account the two-photon excitation effect. The illumination PSF of the one-photon excited spot illumination with different beam widths at the objective pupil is shown in Fig. 4-8. For the calculation, an excitation wavelength of 800 nm is used. The illumination PSF of two-photon excited spot illumination with the excitation wavelength of 800 nm is also shown in Fig. 4-9. Spot-illumination is effective to suppress the out-of-focus in the image. Furthermore, the use of two-photon excitation effectively expands the axial resolution.

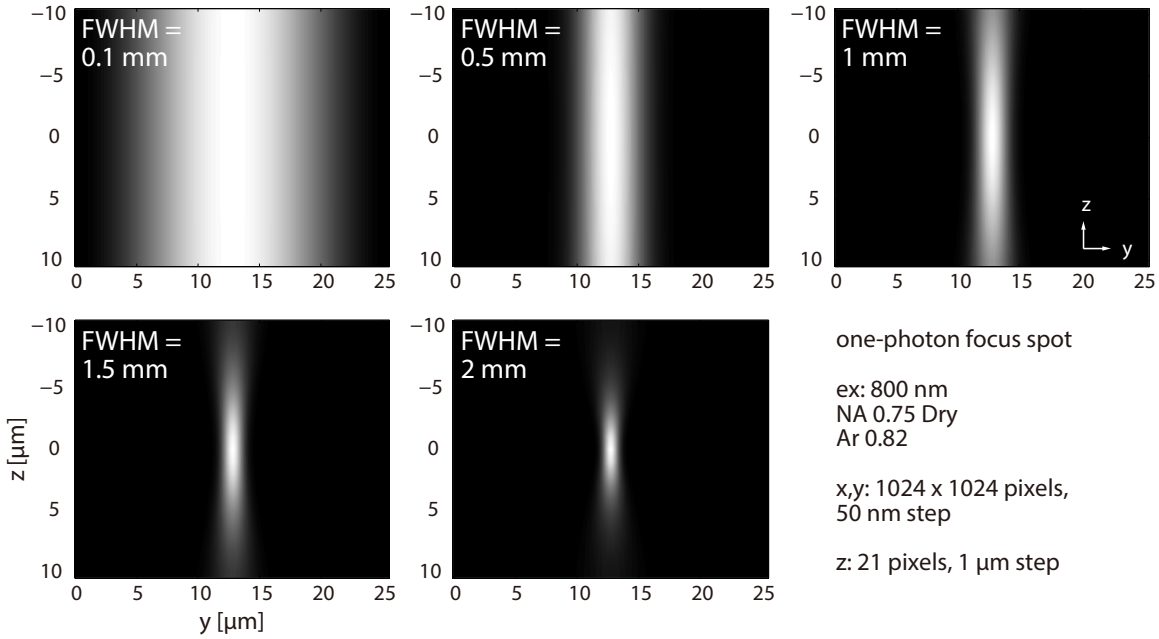

Fig. 4-8 The intensity distribution of the focus spot by NIR one-photon excitation in yz plane with different beam width at the objective pupil.

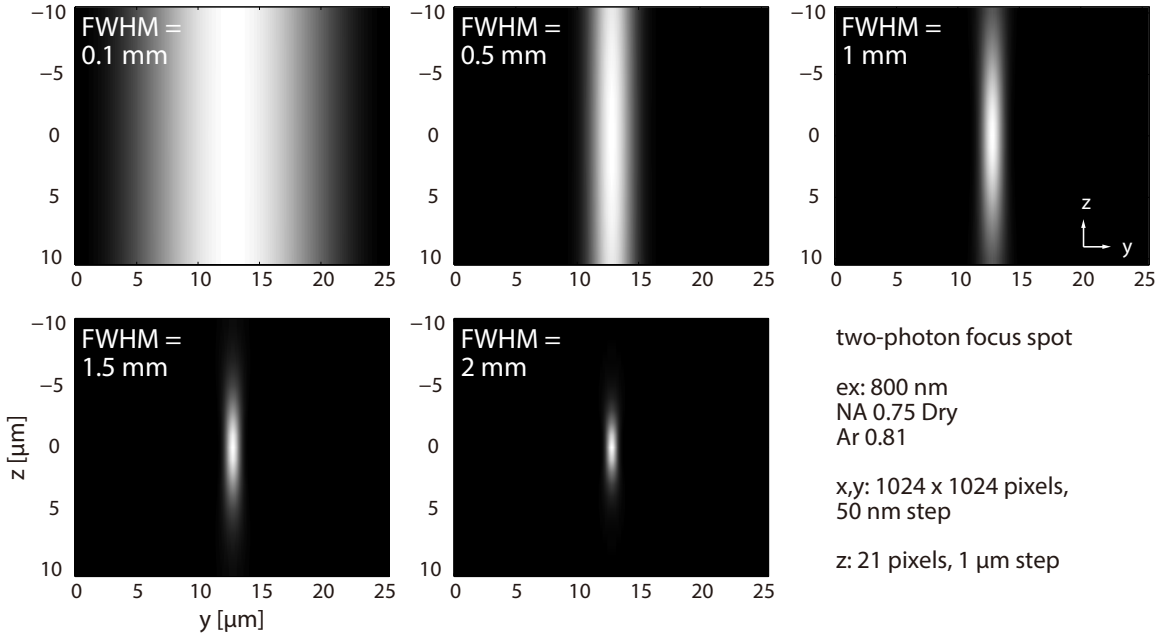

Fig. 4-9 The intensity distribution of the focus spot by NIR two-photon excitation in yz plane with different beam width at the objective pupil.

Fig. 4-10 shows the effective OTF with the different beam width at the objective pupil with the excitation wavelength of 800 nm and detection wavelength of 518 nm. It can be seen that the two-photon spot-SIM with the excitation wavelength of 800 nm has almost the

same axial resolution with the one-photon spot-SIM with the excitation wavelength of 473 nm is shown in Fig. 4-7.

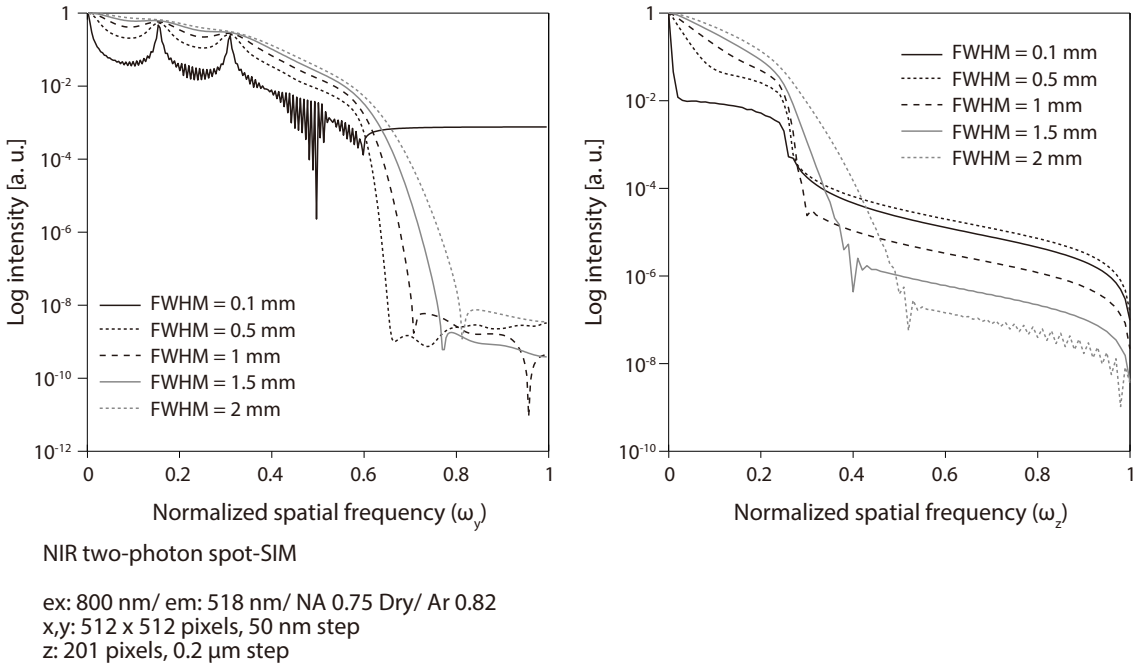

Fig. 4-10 The effective OTF of NIR two-photon spot-SIM in z and y axis with different beam width at the objective pupil.

Fig. 4-11 shows the two-photon spot-SIM OTF under a visible wavelength two-photon excitation condition. The calculation fitting parameter used follows the experimental condition in the reference [11]. The total OTF calculated with the condition shows high axial resolution, as well as lateral resolution.

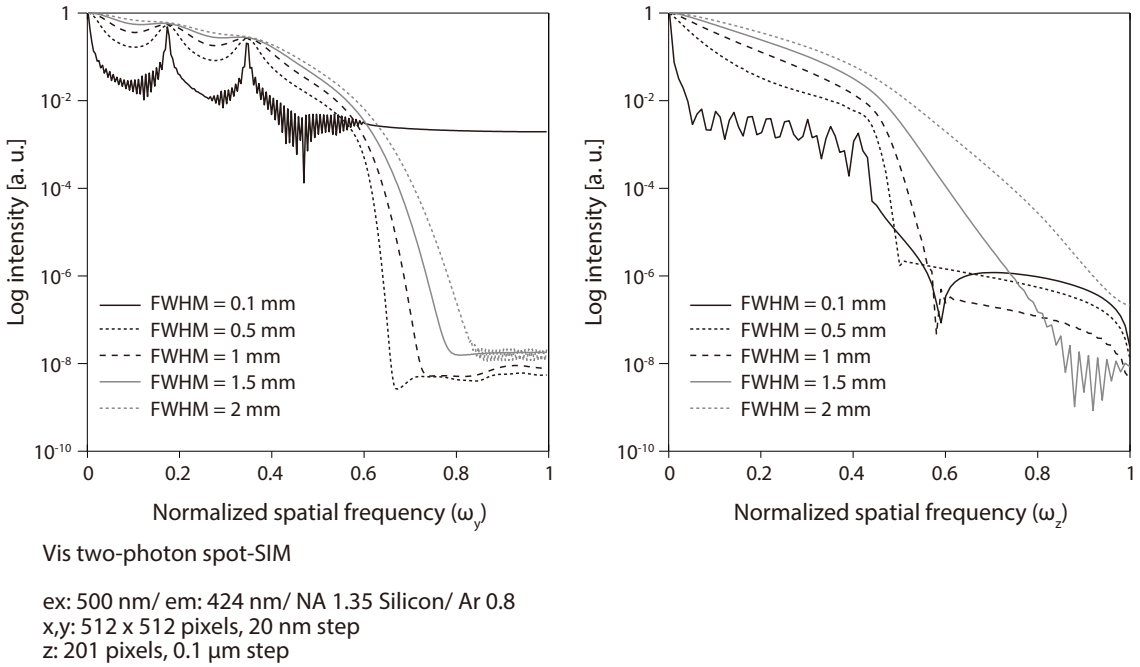

Fig. 4-11 The effective OTF of visible wavelength two-photon spot-SIM in x-z plane with different beam width at the objective pupil.

Discussion

In the wide-field SIM experiment, thick fluorescent sample with the thickness larger than ~20 μm is practically difficult, because of the contribution of the out-of-focus fluorescence signal [4]. Fig. 4-12 illustrates the focused spot along the z-axis in one-photon spot-SIM for different values of FWHM at the objective pupil. For the calculation, the excitation wavelength of 473 nm and detection wavelength of 515 nm, and a NA0.75 x40 dry objective lens are used. In this case, it can be seen that the use of the FWHM at the objective pupil below 1 mm greatly reduces the contribution of out-of-focus light. The z-FWHM of illumination focus spot at sample decreases to 14 μm with the spot size of 1 mm at the objective pupil, which corresponds to the x-FWHM of the focus spot size of 1.2 μm at the sample plane. Therefore, it might be reasonable choice to use the focus spot with the FWHM of ~1.2 μm for the thick fluorescent sample imaging.

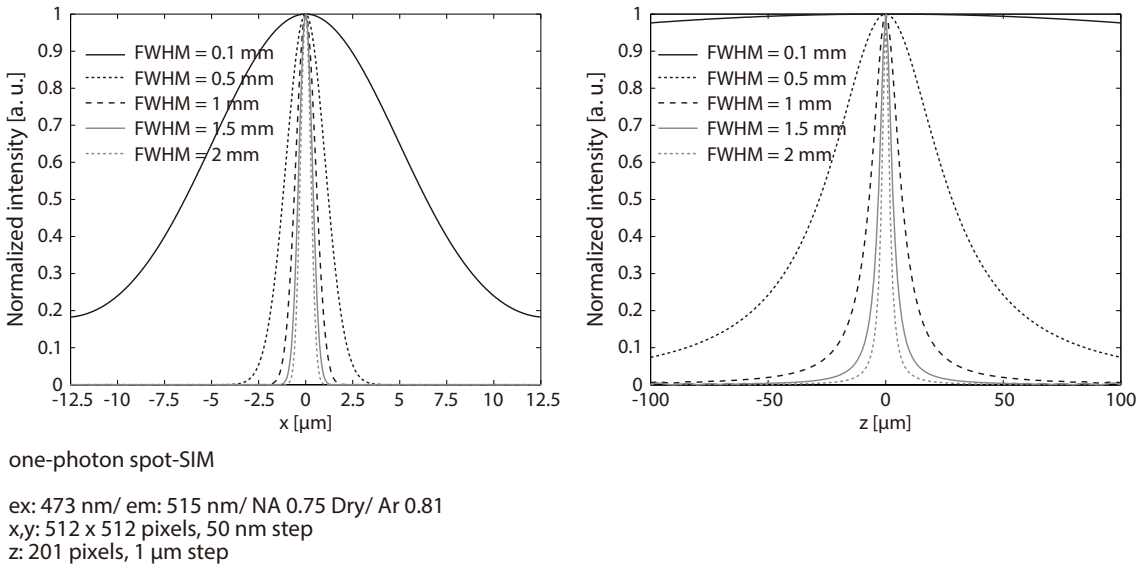

Fig. 4-12 x- and z-profiles of illumination focus spot with different FWHM beam size at the objective pupil.

The determination of the beam width is the trade-off between resolution enhancement and imaging speed. The advantage of wide-field SIM is the imaging speed over the other super-resolution imaging methods, which is slower by the scanning of the illumination pattern. Therefore, it is possible to determine the illumination pattern by the target sample, and to choose the required axial resolution and the imaging speed of the target biological reaction.

References

[1] M. a Neil, R. Juskaitis, and T. Wilson, "Method of obtaining optical sectioning by using structured light in a conventional microscope.," *Opt. Lett.*, vol. 22, no. 24, pp. 1905–7, Dec. 1997.

[2] S. W. Hell, E. H. Stelzer, S. Lindek, and C. Cremer, "Confocal microscopy with an increased detection aperture: type-B 4Pi confocal microscopy.," *Opt. Lett.*, vol. 19, no. 3, p. 222, Feb. 1994.

[3] M. G. L. Gustafsson, D. A. Agard, and J. W. Sedat, "I 5 M: 3D widefield light microscopy with better than 100 nm axial resolution," *J. Microsc.*, vol. 195, no. July, pp. 10–16, 1999.

[4] O. Mandula, M. Kielhorn, K. Wicker, G. Krampert, I. Kleppe, and R. Heintzmann, "Line scan--structured illumination microscopy super-resolution imaging in thick fluorescent samples.," *Opt. Express*, vol. 20, no. 22, pp. 24167–74, Oct. 2012.

[5] S. W. Hell, S. J. Sahl, M. Bates, X. Zhuang, R. Heintzmann, M. J. Booth, J. Bewersdorf, G. Shtengel, H. Hess, P. Tinnefeld, A. Honigmann, S. Jakobs, I. Testa, L. Cognet, B. Lounis, H. Ewers, S. J. Davis, C. Eggeling, D. Klenerman, K. I. Willig, G. Vicidomini, M. Castello, A. Diaspro, and T. Cordes, "The 2015 super-resolution microscopy roadmap," *J. Phys. D. Appl. Phys.*, vol. 48, no. 44, p. 443001, 2015.

[6] T. A. Planchon, L. Gao, D. E. Milkie, M. W. Davidson, J. A. Galbraith, and G. Catherine, "Rapid three-dimensional isotropic imaging of living cells using Bessel beam plane illumination Supplementary figures and tables:," *Nat. Methods*.

[7] A. G. York, S. H. Parekh, D. D. Nogare, R. S. Fischer, K. Temprine, A. B. Chitnis, C. A. Combs, and H. Shroff, "Resolution doubling in live , multicellular organisms via multifocal structured illumination microscopy Supplementary Figure 1 , A misaligned pinhole does not degrade resolution in a confocal microscope microscope with different pinhole configurations . W," *Nat. Methods*, vol. 9, no. 7, 2012.

[8] W. Denk, J. H. Strickler, and W. W. Webb, "Two-photon laser scanning fluorescence microscopy.," *Science*, vol. 248, no. 4951, pp. 73–76, 1990.

[9] M. Ingaramo, A. G. York, P. Wawrzusin, O. Milberg, A. Hong, R. Weigert, H. Shroff, and G. H. Patterson, "Two-photon excitation improves multifocal structured illumination microscopy in thick scattering tissue.," *Proc. Natl. Acad. Sci. U. S. A.*, vol. 111, no. 14, pp. 5254–9, May 2014.

[10] M. G. L. Gustafsson, "Nonlinear structured-illumination microscopy: wide-field

fluorescence imaging with theoretically unlimited resolution.," *Proc. Natl. Acad. Sci. U. S. A.*, vol. 102, no. 37, pp. 13081–6, Sep. 2005.

[11] M. Yamanaka, K. Saito, N. I. Smith, Y. Arai, K. Uegaki, Y. Yonemaru, K. Mochizuki, S. Kawata, T. Nagai, and K. Fujita, "Multiphoton fluorescence microscopy of the live kidney in health and disease Multiphoton fluorescence microscopy of the live kidney in health and disease," *J. Biomed. Opt.*, vol. 19, no. 2, p. 020901, 2014.

Chapter 5
Optical system and experimental results of spot-SIM

Spot illumination with SIM has the possibility of the thick fluorescent sample imaging and deep-tissue imaging by NIR two-photon excitation. Here, I developed the spot-SIM with one-photon excitation and two-photon excitation, and show the enhancement of the spatial resolution using the developed system.

5.1 One-photon excited Spot-SIM

Optical system of Spot-SIM

One-photon excitation spot-SIM can be applied for the thin fluorescent sample imaging suppressing the out-of-focus fluorescence contribution by the spot illumination. I developed structured spot illumination microscope with the excitation wavelength of 473 nm. Fig. 5-1 shows the optical system of the spot-SIM. The wavelength of 473 nm CW (continuous wave) laser with linearly polarized light is used for the excitation. I used aperture ratio of 0.82 at the BFP of the objective lens, which makes 1.82 times extension of the cut-off frequency. The incident light is circularly polarized using quarter wave plate, and then diffracted by phase grating. The linear polarizer, which is inserted in the translational and rotational motor together with the phase grating, ensures that the only linearly polarized light parallel to the grating direction pass through the grating so that the highest interference modulation can be obtained. The 0th order diffraction beam is cut by the beam stop, and then the +1st and -1st diffraction light is reflected by the dichroic mirror (LP515, Carl Zeiss) and illuminate the sample using NA0.75 40x Dry objective (PLAN-NEOFLUAR, Carl Zeiss). The spot illumination with interference fringe pattern is formed with the FWHM of ~ϕ5 μm at the sample plane. Fluorescence from the sample is detected by CCD camera (Clara, Andor) through the emission filter (505DRLP). In order to reconstruct high-resolution image, 9 images (3 rotational angles, 3 translation position of the grating) are measured at the same position. The images are acquired with the exposure time of 100 msec.

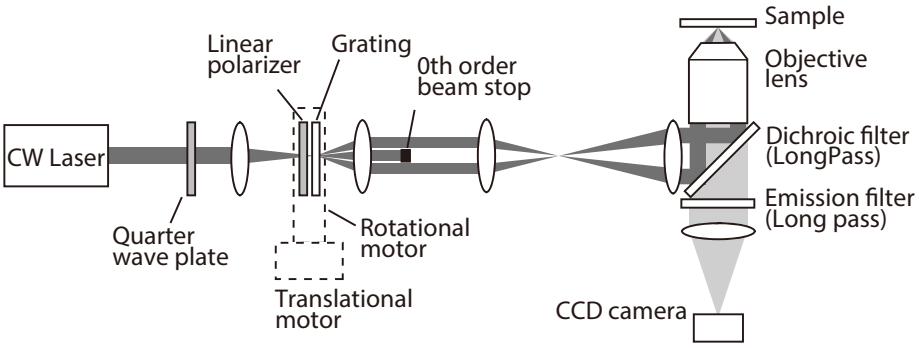

Fig. 5-1 The optical setup of the one-photon excited spot-SIM.

Experimental result of fluorescence beads imaging

Fig. 5-2 shows the data sets, which acquired in described spot-SIM system. The data set is then mathematically processed by the SIM reconstruction software developed by Prof. Heintzmann's group in Institute of photonics technology (biological nanoimaging research group, IPHT, Germany). Here the reconstruction process is briefly explained. The fluorescence intensity fluctuation of each image is normalized, and the position drift error is corrected. The subsequent iterative calculations define the position and the modulation depth of the SI peaks. The frequency components are then extracted by iterative calculation. After applying linear Wiener filter, both wide-field like and high-resolution SIM image are constructed.

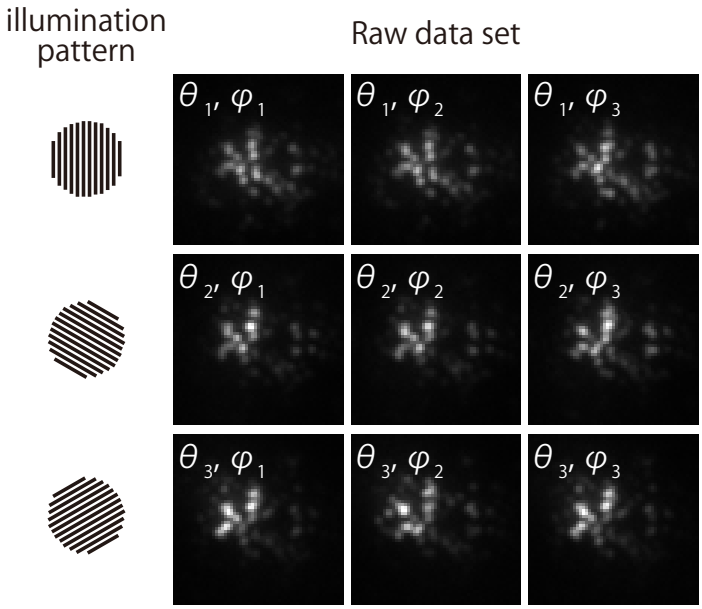

Fig. 5-2 Raw data sets of fluorescence beads image in spot-SIM

The reconstructed spot-SIM image shows clear spatial resolution improvement compared to the reconstructed wide-field-like image. Fig. 5-3 shows the spot illumination and spot-SIM image of fluorescence beads with the diameter of 0.1 μm, whose excitation peak at 470 nm and fluorescence emission peak at 480 nm (Krister Biotech GmbH & Co. KG, Germany). The profile of the one isolated fluorescence bead shows the smaller PSF of the spot-SIM than spotlight microscopy. In addition, the two-point resolution is clearly improved, which is seen in the profiles of two adjacent fluorescence particles.

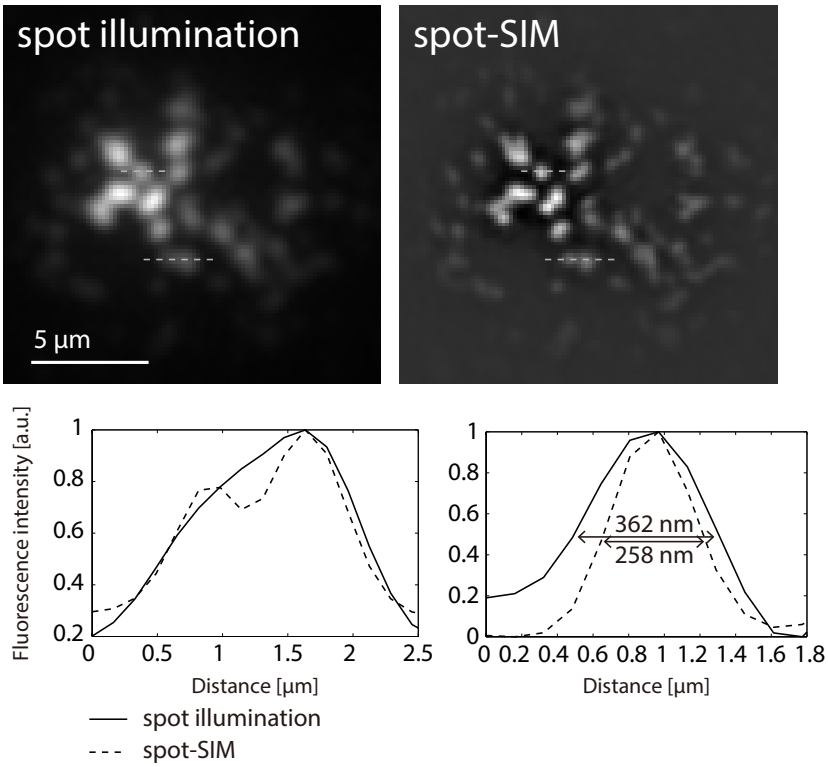

Fig. 5-3 Comparison of spotlight image and spot-SIM image

Discussion

The acquisition speed has to be faster for the practical application of spot-SIM. In this experiment, it is needed to take ~30 sec for the acquisition of one dataset, which is much slower than the general SIM with the maximum flame rate of 7.6 per sec [1]. Optimizing the mechanical system or utilizing the polarization property of light can overcome this problem. One possibility to increase the flame rate by the optimization of the mechanical system is that

replacing the translational DC motor, which is used for the phase shift of the grating, to a piezo stage, since the slow movement of the DC motor restricts the acquisition speed of the current system. Another possibility is to use DMD (Digital mirror device) or SLM (Spatial light modulator) instead of physical grating to diffract the incident light. Fast SIM using SLM is reported, and this approach can provide much faster image acquisition speed. As another approach for the fast SIM using polarization is also reported [2]. Using different polarization for the illumination pattern, one can obtain different illumination phase images at the same time. Increasing the acquisition speed by combining these methods can be also possible.

5.2 Two-photon excited spot-SIM for deep-tissue imaging

Optical system of two-photon spot-SIM

Two-photon spot-SIM can further improve the applicability of spot-SIM to deep tissue imaging. For the deep tissue imaging of the biological specimen, NIR pulse laser is generally used for the excitation laser for its long penetration depth in the tissue. The experimental setup of the two-photon spot-SIM is shown in Fig. 5-4. I used Ti:Sapphire laser with the pulse width of 140 fs, repetition rate of 80 MHz and wavelength of 800 nm (Chameleon Ultra II). The laser power output is kept to 3 W and 30 % of the power is goes through the optics after the beam splitter, which is placed in front of the laser exit. The polarization of the system is maintained by the same way with the one-photon case, which is described in chapter 5.1. The aperture ratio (Ar) of 0.81 at the BFP of the objective lens is used for the illumination. The incident light is reflected by the short-pass dichroic mirror (650DRSP, Bjomejag) and the spot illumination with interference fringe pattern with the illumination area of ~ϕ25 μm is formed at the sample plane. Fluorescence signal from the sample is detected by CCD camera (iXon Ultra 897, Andor) with the external magnification of 2.5x, through the two emission filters (BP505-530, Carl Zeiss; Bright Line533, Semrock) for the effectively suppressing the intense reflection light. In order to reconstruct high-resolution image, 15 images (3 rotational angles, 5 translation position of the grating) are measured at the same position, in order to treat with the 2nd order peaks appeared by the effect of non-linear excitation. The images are acquired with the exposure time of 500 msec.

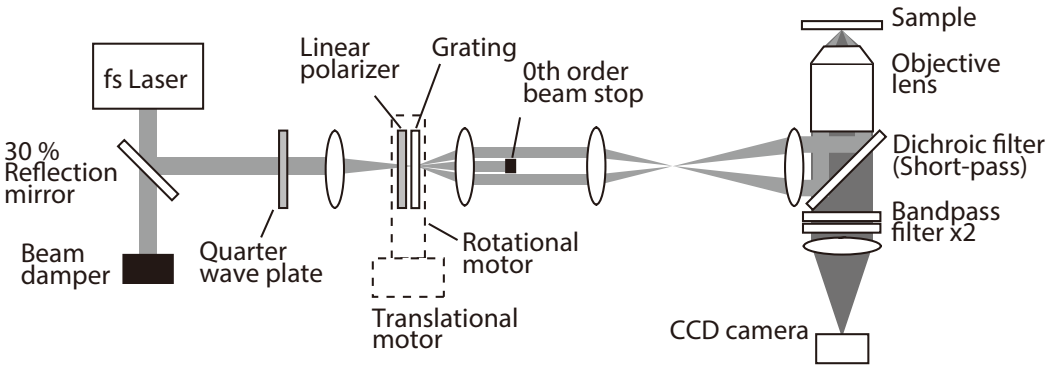

Fig. 5-4 The optical setup of the two-photon excited spot-SIM

Experimental result of fluorescence beads imaging

Fig. 5-5 shows the raw data set that is obtained from the imaging of fluorescence particles with the diameter of 0.1 μm with the excitation and emission peak at 470 nm and 480 nm, respectively (Krister Biotech GmbH & Co. KG, Germany). The images are reconstructed by the same calculation software, which is used for the one-photon spot-SIM.

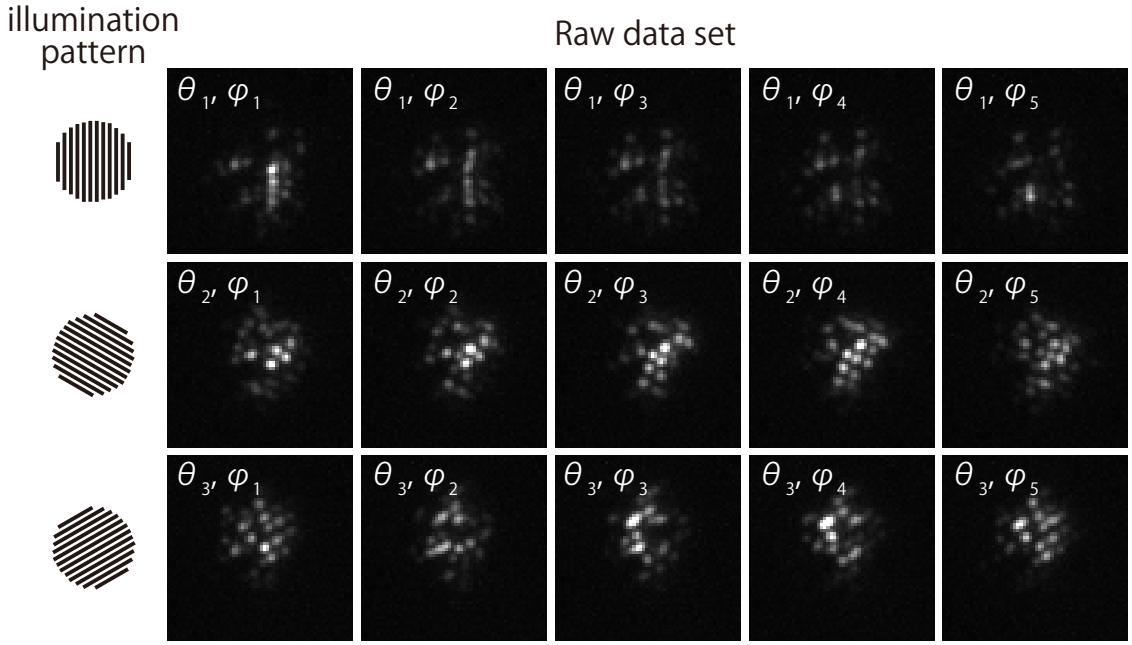

Fig. 5-5 Raw data set used for the reconstruction of one high-resolution two-photon spot-SIM image.

The reconstructed two-photon spot-SIM image shows clear spatial resolution

improvement compared to the reconstructed wide-field-like image. Fig. 5-6 shows the spotlight and spot-SIM image of fluorescence beads with the diameter of 0.1 μm. The profile of the one isolated fluorescence bead shows the smaller PSF of the spot-SIM than spotlight microscopy. The profiles of isolated fluorescence particle show clear spatial resolution improvement in spot-SIM. The two-point resolution is also clearly improved, which is seen in the profiles of two adjacent fluorescence particles.

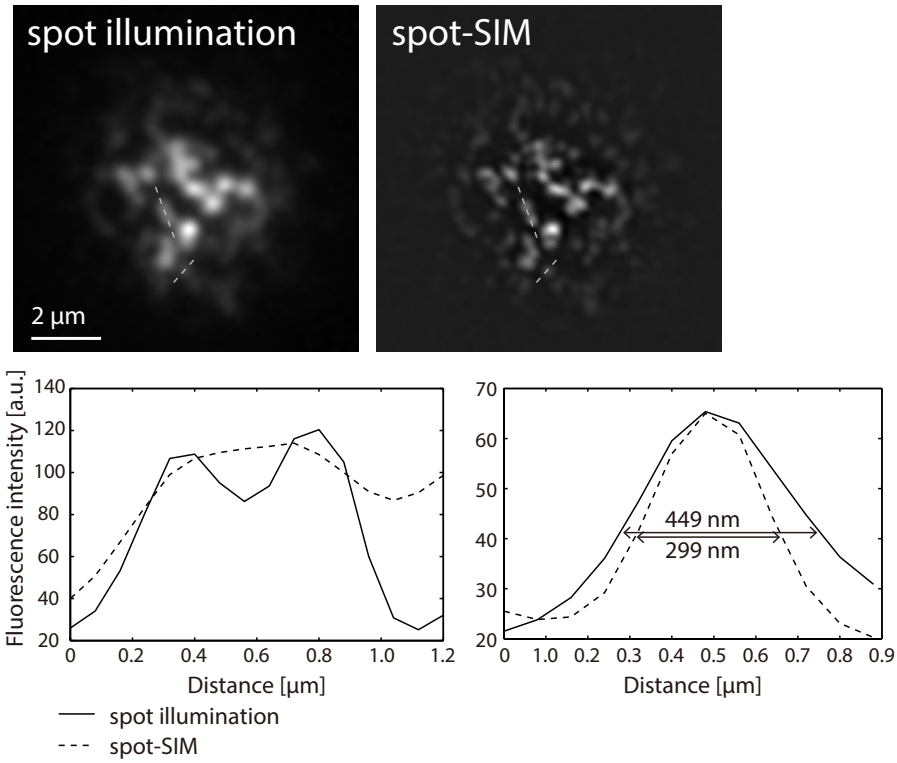

Fig. 5-6 The resolution improvement by two-photon spot-SIM can be seen by the comparison of spot illumination microscopy and spot-SIM.

Discussion

The excitation wavelength of longer than 800 nm will improve the penetration depth for the practical application of two-photon spot-SIM to deep-tissue imaging. For example GFP, which provides strong fluorescence signal, has the absorption peak at 488 nm; therefore, excitation wavelength of 1000 nm may provide higher signal, thus higher SNR. For the practical application of this microscopy, wavelength select ability with tunable wavelength laser and dichroic filter and emission filter is desired for optimizing the parameter for each measurement.

In this experiment, I used relatively large illumination spot in order to ensure the overlap of the illumination area with different illumination angle, in order to experimentally demonstrate the applicability of SIM strategy to spot illumination. However, as it can be seen from the calculation of the illumination spot size in chapter 4, it is desirable to use spot size with ~1-2 μm to effectively suppress the out-of-focus signal. For the actual application of the spot-SIM to the biological sample, the spot-SIM setup with small spot size and illumination scanning system is the desired choice.

Two-photon microscopy with spot illumination was studied by J. Y. Hwang in 2011, which provides faster imaging speed comparing with general point-scanning two-photon microscopy system [3]. In their study, they used illumination spot of ~ϕ50 μm to ensure the higher imaging speed, and successfully obtained the two-photon imaging of the fluorescence beads sample under the maximum 17 μm beneath the mouse skin in vivo. According to the calculation, the two-photon spot-illumination imaging with the spot size of ϕ50 μm may only provide the illumination z FWHM of ~50 μm. Therefore, in our strategy, it is possible to use smaller illumination area to suppress the out-of-focus signal effectively, to visualize much deeper structure in biological tissue.

Our spot-SIM setup can be further expand to three dimensional super-resolution imaging using 3D SIM strategy [4]. The use of three-beam interference setup enables to achieve the excitation interference pattern in axial direction. Therefore, extraction of the information from three dimensionally structured illumination pattern enables high-resolution imaging in both lateral and axial direction.

References

[1] R. Förster, H.-W. Lu-Walther, A. Jost, M. Kielhorn, K. Wicker, and R. Heintzmann, "Simple structured illumination microscope setup with high acquisition speed by using a spatial light modulator.," *Opt. Express*, vol. 22, no. 17, pp. 20663–77, Aug. 2014.

[2] K. Wicker and R. Heintzmann, "Single-shot optical sectioning using polarization-coded structured illumination," *J. Opt.*, vol. 12, no. 8, p. 084010, Aug. 2010.

[3] J. Y. Hwang, S. Wachsmann-hogiu, V. K. Ramanujan, G. Nowatzyk, Y. Koronyo, L. K. Medina-kauwe, Z. Gross, H. B. Gray, and D. L. Farkas, "Multimodal wide-field two-photon excitation imaging: characterization of the technique for in vivo applications," *Biomed. Opt. Express*, vol. 2, no. 2, pp. 253–259, 2015.

[4] M. G. L. Gustafsson, L. Shao, P. M. Carlton, C. J. R. Wang, I. N. Golubovskaya, W. Z. Cande, D. a Agard, and J. W. Sedat, "Three-dimensional resolution doubling in wide-field fluorescence microscopy by structured illumination.," *Biophys. J.*, vol. 94, no. 12, pp. 4957–70, Jun. 2008.

Conclusions

In this study, I developed scanning structured illumination microscopy in order to realize high-resolution label-free imaging or deep-tissue imaging. SIM is one of the high-resolution optical microscopy techniques, which has the potential for the high-speed and high-resolution optical imaging. Moreover, SIM can be applied to the non-fluorescent label-free imaging or thick fluorescent sample imaging, because the resolution enhancement of the SIM doesn't rely on the non-linear fluorescence property or precise control of the fluorescence emission capabilities. The combination of SIM with scanning of illumination shows extended availability of the SIM to image the sample, which cannot be imaged in current optical microscopy technique.

The application of the SIM to line illumination has the potential to realize the spectral imaging. In chapter 2, the image formation of the SLI microscopy and the calculated OTF with different illumination conditions are presented. In chapter 3, the practical development of the SLI Raman microscopy is shown. The resultant SLI microscope image shows clear spatial resolution improvement for polymer nanoparticles, graphene, graphite, mouse brain tissue, and fixed HeLa cell imaging. Our SLI Raman microscope shows good balances between image acquisition speed and spatial resolution enhancement in lateral direction.

For the further improvement of the spatial resolution, it is required to optimize the optics, since the spatial resolution in the current setup seems to be degraded by the aberrations induced by the multiple optical relays and the optics inside the spectrophotometer. Solving these problems in the optical system, it may be possible to achieve spatial resolution lower than 150 nm, which will further expands the possibility of the Raman microscopy for the micro-spectroscopy of the nano-structured samples.

In chapter 4, the application of the SIM to spot illumination is discussed, and the theoretical calculations are conducted to show the increased ability of the SIM for the optically sectioned imaging. I constructed spot-SIM system and revealed resolution enhancement with one-photon and NIR excited two-photon microscopy (chapter 5). The developed microscope shows the enhanced spatial resolution in lateral direction. The successfully constructed spot-SIM setup may show the actual availability of the SIM toward high-resolution deep tissue imaging.

Although I showed the possibility of the spot-SIM to the application of high-resolution and high-speed deep-tissue imaging, the experimental verification of the axial resolution is needed for the future study. For the practical application of the microscope, it is required to implement the scanning system, with the optimized for high-speed imaging and also the spot-size should be optimized to fit for the thickness of the target sample.

The combination of the SIM with laser-scanning microscopy expands the possibilities of high-resolution microcopy techniques to spectral and non-linear imaging. As discussed in the chapter 1, super-resolution imaging has been invented several tens years ago, and now the technique is reaching to the high-resolution video-rate imaging level. The recent development of the super-resolution microscopy, as well as the new possibility of the optical imaging methods provided in here, will be expected to have significant important to the actual application to the biological and industrial optical imaging.

List of Publications

Original paper

1. K. Watanabe, A. F. Palonpon, N. I. Smith, L. Chiu, A. Kasai, H. Hashimoto, S. Kawata and K. Fujita, ”Structured line illumination Raman microscopy”, *Nature Communications* 6:10095 doi: 10.1038/ncomms10095 (2015)
2. K. Watanabe, K. Fujita, S. Kawata and R. Heintzmann, “Two-photon excitation microscopy with structured spot illumination for high-resolution imaging of thick fluorescent samples”, in preparation

International conferences

1. K. Watanabe, A. F. Palonpon, N. I. Smith, L. Chiu, A. Kasai, H. Hashimono, S. Kawata and K. Fujita, “Raman microscopy using structured line illumination” *Focus on Microscopy*, Gottingen, Germany, March, 2015.
2. K. Watanabe, A. F. Palonpon, N. I. Smith, L. Chiu, A. Kasai, H. Hashimono, S. Kawata and K. Fujita, “Resolution improvement of Raman microscopy by structured line illumination” *Japan-Morocco Handai project on functional nanophotonics Kick-off workshop*, Rabat, Morocco, February, 2015.
3. K. Watanabe, L. Chiu, A. F. Palonpon, S. Kawata and K. Fujita, “Raman microscopy for high-resolution vibrational imaging” *Japan Taiwan bilateral conference on biomedical and plasmonic imaging*, Taipei, Taiwan, February, 2014.

Scholarship and Grant

1. 渡辺梢、 「研修交流助成【海外研修】」 公益財団法人中谷医工計測技術振興財団（2015）
2. 日本学術振興会特別研究員（DC2）
3. 大阪大学大学院工学研究科リサーチアシスタント（GCOE）

Acknowledgement

I would like to express my deepest gratitude to Prof. Satoshi Kawata for accepting me as a PhD student in his group. I appreciate his hearty encouragement to my life and supervising my study though PhD course to keep the positive attitude to my study.

My best gratitude goes to Prof. Katsumasa Fujita for his greatest supervision of my study and the encouragement to pursue the PhD. My PhD study has accomplished with his scientific supports and also moral encouragements.

I would also appreciate the support by Prof. Nicholas I. Smith for giving me constructive and technical advices. The clear perspectives toward the physical and biological phenomena always helped me to learn a lot from the discussion and experimental results.

I would like to express my gratefulness to Prof. Hitoshi Hashimoto and Prof. Atsushi Kasai for helping the biological part of out study.

I would like to show my thankfulness to Prof. Yasushi Inouye, Prof. Eichi Tamiya, and Prof. Yasushi Okada for kindly reviewing the thesis and giving me fruitful suggestions and comments.

I would like to express my best gratefulness to Dr. Almar F. Palonpon for always giving me critical and constructive way of thinking in science and how to express the scientific achievement. I learned not only the experimental and theoretical study of microscopy, but also the moral attitude as a scientist. My best gratefulness also goes to Dr. Liang-da Chiu for giving me the first guidance during the PhD study. Thank you so much for encouraging me to pursue myself to be an independent scientist.

I would also show my deepest thankfulness to Prof. Heintzmann for supervising me as an international student in his group. I understand the idea of the SIM much more deeply through the stay in Jena, and impressed by his kind hospitality.

I would like to show my thankfulness to former and present colleagues in LaSIE, Kyoko Masui, Jun Ando, Masahito Yamanaka, and Yasuaki Kumamoto for kindly giving advices. I would also express my thankfulness to former and present students in LaSIE, especially Masaya Okada, Yasuo Yonemaru, Kentaro Mochizuki, Shota Ushiba, Imad Maouli, Yan Zhao-Xu, Toshihiro Mino, Kazuki Bando, Yoshiro Ohashi, and Takayuki Umakoshi. I was motivated by the scientific discussion and also enjoyed holding student chapter activities, which I couldn't experience without them.

I express my gratefulness to friends, who I met during the lab life, especially Mei-Yu Chen, Li-Chuan Huang, René Richter, Ronny Förster and Robert Kretchmer. I learned the positive attitude toward my study as well as my life. I would also thank to all of the members in LaSIE, and biological nanoimaging research group in Jena for helping me a lot.

Finally, I would like to express my best acknowledgement to my family and my friends. Best thankfulness goes to Shigeru Watanabe, Marie Watanabe, Maiko Watanabe, and Nobuko Akiyama for always cheering me up to pursue what I should do. I also express my deepest thankfulness to Maasa Nakano, Yurika Yoshida, Aki Yazawa, and Shiori Waki for their continuous encouragement and support.